February 25, 2005

Selection and study of the $B_s^0 \to D_s^- \pi^+$ decay at LHCb

Master Thesis

Louis Nicolas [1]

Laboratory for High-Energy Physics (LPHE)
Swiss Federal Institute of Technology Lausanne (EPFL)

Directed by Prof. Olivier Schneider [2]
Assisted by Luis Fernández [3] and Dr Jeroen van Hunen [4]

[1] louis.nicolas@epfl.ch
[2] olivier.schneider@epfl.ch
[3] luis.fernandez@epfl.ch
[4] jeroen.vanhunen@epfl.ch

Abstract

The decay channel $B_s^0 \to D_s^- \pi^+$ will be used in LHCb to extract the physics parameters ΔM_s and $\Delta\Gamma_s$ and the wrong tag fraction ω. This flavour specific decay may also serve as a control channel for $B_s^0 \to D_s^\pm K^\mp$ which is used to extract the CP-violating phases $\gamma+\phi_s$. This study of fully Monte Carlo simulated events shows that an annual signal yield of (111.4 ± 0.5)k reconstructed, triggered and selected events can be obtained. The background-to-signal ratio for this channel is expected to be (0.83 ± 0.09) where the dominant source of background is assumed to be $b\bar{b}$. The effective combined tagging efficiency is expected to be $(6.10 \pm 0.19)\%$.

The proper time resolution is also investigated and a value of 41.8 fs is found. This resolution is dominated by the spatial resolution on the B_s-decay vertex. This is still a very good resolution which will allow to resolve the fast B_s^0-$\bar{B}_s^0$ oscillations

The efficiency of selection is analysed as a function of the true proper time before and after trigger. The results show that this efficiency is smaller for low proper times (due to the cuts requiring a displaced secondary vertex) and is also decreasing for large proper time. This effect is found to be enhanced by the Level-0 trigger and even more by the Level-1 trigger.

Finally, the sensitivity to ΔM_s is calculated and the analysis shows that this parameter will be measurable (with a statistical significance of at least 5σ) up to 46 ps^{-1}.

Contents

List of Tables

List of Figures

1 Introduction

1.1 Particle physics and CP violation

CP violation was first discovered in neutral K-meson decays in 1964 [1]. Other systems of interest in this field are the neutral D meson and B mesons. In this chapter the theory of CP violation [2] and the Standard Model (SM) will be briefly described.

C, P and T are the three discrete symmetries. P is the parity and represents a space inversion, reversing the handedness. T represents the time reversal, interchanging the forward and backward light-cones. The third discrete operation is the charge conjugation, C, which interchanges particles and antiparticles. The combination CP replaces a particle by its antiparticle and reverses momentum and helicity. The combination CPT is an exact symmetry in any local field theory.

It has been observed that electromagnetic and strong interactions are invariant under the P, C and T transformations. The weak interaction violates C and P separately, but preserves CP and T to a good approximation. Only certain rare processes have been observed to exhibit CP violation. All observations to date are consistent with exact CPT symmetry.

The Standard Model (SM) with three quark families can naturally generate CP violation in the weak interaction. In this model, flavour changing processes between the quarks are only due to charged current interactions with couplings given by the elements of a 3×3 unitary matrix, usually referred to as the Cabibbo-Kobayashi-Maskawa (CKM) matrix. The CKM matrix connects the electroweak eigenstates (d', s', b') to their corresponding mass eigenstates (d, s, b):

$$\begin{pmatrix} d' \\ s' \\ b' \end{pmatrix} = \mathbf{V}_{\mathrm{CKM}} \begin{pmatrix} d \\ s \\ b \end{pmatrix} \quad ; \quad \mathbf{V}_{\mathrm{CKM}} = \begin{pmatrix} V_{ud} & V_{us} & V_{ub} \\ V_{cd} & V_{cs} & V_{cb} \\ V_{td} & V_{ts} & V_{tb} \end{pmatrix}.$$

This matrix can be parametrised with four independent parameters, including a complex phase, which introduces CP violation. A convenient parametrisation for phenomenology, introduced by Wolfenstein [3], is given in terms of the expansion of the small quantity λ together with the parameters (ρ, η, A). $\mathbf{V}_{\mathrm{CKM}}$ can here be approximated as

$$\mathbf{V}_{\mathrm{CKM}} \approx \begin{pmatrix} 1-\lambda^2/2 & \lambda & A\lambda^3(\rho - i\eta) \\ -\lambda & 1-\lambda^2/2 & A\lambda^2 \\ A\lambda^3(1-\rho-i\eta) & -A\lambda^2 & 1 \end{pmatrix} + \delta\mathbf{V}_{\mathrm{CKM}} \qquad (1)$$

where

$$\delta\mathbf{V}_{\mathrm{CKM}} = \begin{pmatrix} 0 & 0 & 0 \\ -iA^2\lambda^5\eta & 0 & 0 \\ A\lambda^5(\rho+i\eta)/2 & A\lambda^4(1/2-\rho-i\eta) & 0 \end{pmatrix} \qquad (2)$$

includes the next-to-leading orders in $\lambda \equiv \sin(\theta_C)$, where θ_C is the Cabibbo angle ($\sin(\theta_C) = 0.2243 \pm 0.0016$ [22], using the measurements done so far in various experiments). CP violation occurs when $\eta \neq 0$, i.e. when the CKM matrix is complex.

The unitarity of the CKM matrix leads to a set of 6 orthogonality relations that can be represented as triangles in the complex plane. The angles of these triangles correspond to the weak phases that need to be investigated in order to test the CKM picture.

The CKM matrix can be parametrised as four independent phases; a convenient choice is given by:

$$\beta \equiv \arg\left(-\frac{V_{cd}\,V_{cb}^*}{V_{td}\,V_{tb}^*}\right) \equiv \beta_d \approx 23.8^\circ, \tag{3}$$

$$\gamma \equiv \arg\left(-\frac{V_{ud}\,V_{ub}^*}{V_{cd}\,V_{cb}^*}\right) \approx 62^\circ \quad \text{or} \quad \alpha \equiv \arg\left(-\frac{V_{td}\,V_{tb}^*}{V_{ud}\,V_{ub}^*}\right) \approx 94^\circ \tag{4}$$

$$\beta_s \equiv \arg\left(-\frac{V_{cb}\,V_{cs}^*}{V_{tb}\,V_{ts}^*}\right) \equiv \chi \tag{5}$$

$$\beta_k \equiv \arg\left(-\frac{V_{us}\,V_{ud}^*}{V_{cs}\,V_{cd}^*}\right) \equiv \chi'. \tag{6}$$

These angles appear in the following triangles:

$$\underbrace{V_{ud}V_{ub}^*}_{(\rho+i\eta)A\lambda^3} + \underbrace{V_{cd}V_{cb}^*}_{-A\lambda^3} + \underbrace{V_{td}V_{tb}^*}_{(1-\rho-i\eta)A\lambda^3} = 0 \quad (bd-\text{triangle}) \tag{7}$$

$$\underbrace{V_{ud}^*V_{td}}_{(1-\rho-i\eta)A\lambda^3} + \underbrace{V_{us}^*V_{ts}}_{-A\lambda^3} + \underbrace{V_{ub}^*V_{tb}}_{(\rho+i\eta)A\lambda^3} = 0 \quad (ut-\text{triangle}) \tag{8}$$

$$\underbrace{V_{us}V_{ub}^*}_{\mathcal{O}(\lambda^4)} + \underbrace{V_{cs}V_{cb}^*}_{\mathcal{O}(\lambda^2)} + \underbrace{V_{ts}V_{tb}^*}_{\mathcal{O}(\lambda^2)} = 0 \quad (bs-\text{triangle}) \tag{9}$$

$$\underbrace{V_{ud}V_{us}^*}_{\mathcal{O}(\lambda)} + \underbrace{V_{cd}V_{cs}^*}_{\mathcal{O}(\lambda)} + \underbrace{V_{td}V_{ts}^*}_{\mathcal{O}(\lambda^5)} = 0 \quad (sd-\text{triangle}) \tag{10}$$

Only two triangles, bd and ut, have all three sides of comparable size ($\mathcal{O}(\lambda^3)$). Moreover the two triangles, shown in Fig. 1), agree at the λ^3 level consequently describing the same triangle, which is referred to as "the" unitarity triangle of the CKM matrix. The bd triangle (Eq. (7)) is of particular interest for the B_d^0-system since it contains the CKM factors involved in the B_d^0-decays.

All the other triangles, such as bs and sd, have one side Cabibbo suppressed and are thus squashed. The bs triangle is the strange counterpart of the unitarity triangle and is therefore relevant for the B_s^0 system, whereas the sd triangle will describe CP violation in the K^0 system.

The amplitude of the oscillations of the B_d^0-$\bar{B}_d^0$ and the B_s^0-$\bar{B}_s^0$ systems will be controlled by the phases of the box diagrams (Fig. 2 a)):

$$\phi_d = 2\arg[V_{td}^*V_{tb}] \approx 2\beta_d\ , \tag{11}$$

$$\phi_s = 2\arg[V_{ts}^*V_{tb}] \approx -2\beta_s \approx -2\lambda^2\eta \sim \mathcal{O}(-0.04)\ \text{rad}. \tag{12}$$

Finally Wolfenstein's parametrisation implies

$$\arg V_{td} = -\beta_d, \qquad \arg V_{ub} = -\gamma, \qquad \arg V_{ts} = \beta_s + \pi$$

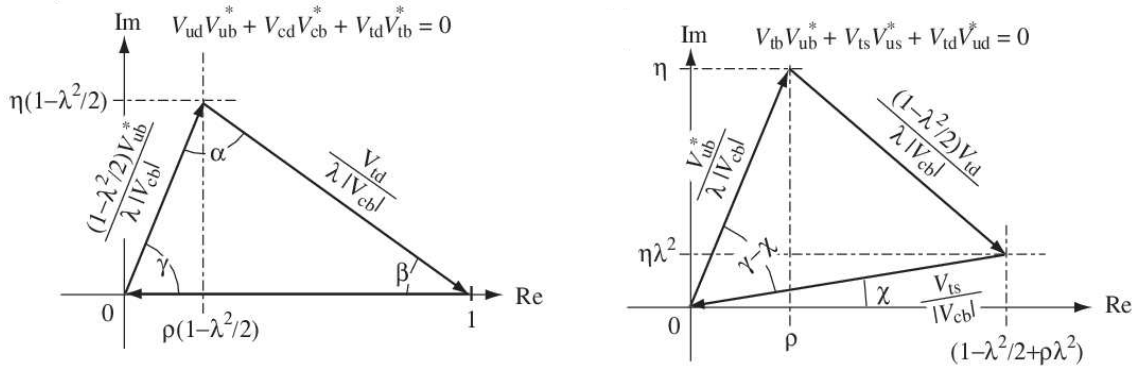

FIG. 1: Two unitarity relations (Eqs. (7) and (8)) drawn in the complex plane.

and that all the other elements are real.

The different CKM factors can be extracted from various B-meson decays.

In absence of the weak interaction, the neutral B_s^0 mesons have well defined flavours. Once the weak interaction is "turned" on, a general state can be written as

$$|\psi(t)\rangle = a(t)|B_s^0\rangle + b(t)|\bar{B}_s^0\rangle + \sum_i c_i(t) f_i,$$

where f_i are the possible final states to which either B_s^0 or $\bar{B}_s^0$ may decay through the weak interaction and t is the time in the B_s^0-$\bar{B}_s^0$ rest frame. At $t = 0$, the B_s^0 states are stable and then start to mix and decay for $t > 0$. Neglecting the interactions between final states, the B_s^0-system can be described by a two-component wave function with an evolution described by the following effective Schrödinger equation:

$$i\frac{d}{dt}\begin{pmatrix} a \\ b \end{pmatrix} = H\begin{pmatrix} a \\ b \end{pmatrix} \equiv \left(M - \frac{i}{2}\Gamma\right)\begin{pmatrix} a \\ b \end{pmatrix}$$

where M and Γ are the 2×2 Hermitian mass and decay matrices respectively. CPT invariance guarantees $H_{11} = H_{22}$. The off-diagonal terms in these matrices, M_{12} and Γ_{12} are particularly important in the discussion of CP violation. They are the dispersive and absorptive parts respectively of the transition amplitude from B_s^0 to $\bar{B}_s^0$.

The B_L and B_H mass (or physical) eigenstates [1] are given by

$$|B_{L/H}\rangle = p|B_s^0\rangle \pm q|\bar{B}_s^0\rangle,$$

where the complex coefficients p and q obey the normalization condition

$$|q|^2 + |p|^2 = 1,$$

and their ratio is given by

$$\frac{q}{p} = -\sqrt{\frac{M_{12}^* - \frac{i}{2}\Gamma_{12}^*}{M_{12} - \frac{i}{2}\Gamma_{12}}}. \tag{13}$$

[1] L and H stand for Light and Heavy respectively

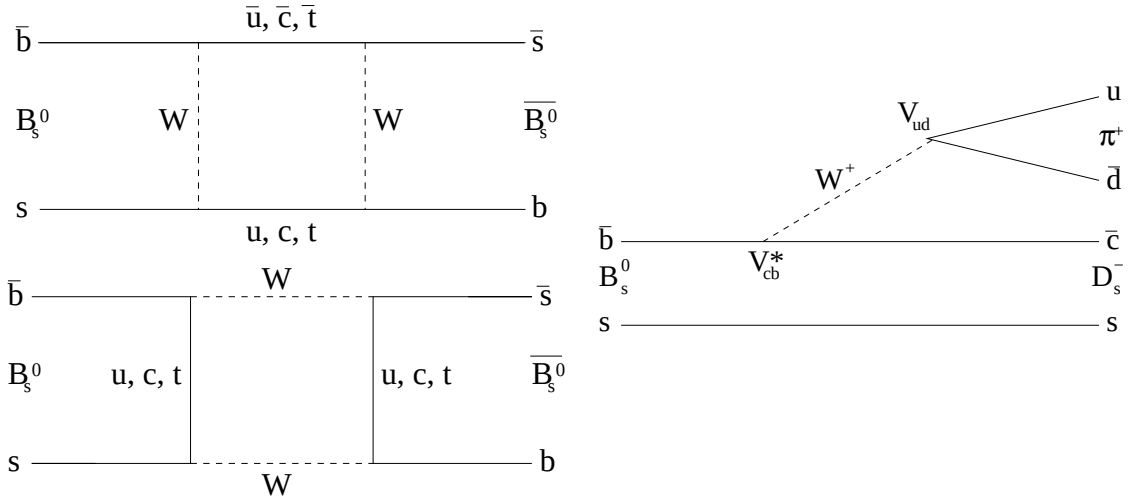

(a) Box diagrams of the $B_s^0 - \bar{B}_s^0$ oscillation,

(b) Tree diagram of the $B_s^0 \to D_s^- \pi^+$ decay.

FIG. 2: Diagrams of interest for the B_s^0-$\bar{B}_s^0$ and for the $B_s^0 \to D_s^- \pi^+$ decay.

The mass difference ΔM_s and width difference $\Delta\Gamma_s$ between the mass eigenstates are defined as:

$$\Delta M_s \equiv M_H - M_L \qquad \Delta\Gamma_s \equiv \Gamma_L - \Gamma_H,$$

so that ΔM_s is positive by definition and with

$$\Delta M_s \sim \mathcal{O}(20)\text{ps}^{-1} \quad , \quad \tau_{B_s} = \frac{1}{\Gamma_s} = 1.46\text{ps}$$

and

$$\Gamma_s = \frac{\Gamma_H + \Gamma_L}{2} \quad , \quad \frac{\Delta\Gamma_s}{\Gamma_s} \sim \mathcal{O}(10\%).$$

The time evolution of initially pure B_s^0 and $\bar{B}_s^0$ meson states is given by

$$|B_s^0(t)\rangle = f_+^{(s)}(t)|B_s^0\rangle + \frac{q}{p} f_-^{(s)}(t)|\bar{B}_s^0\rangle, \tag{14}$$

and

$$|\bar{B}_s^0(t)\rangle = \frac{p}{q} f_-^{(s)}(t)|B_s^0\rangle + f_+^{(s)}(t)|\bar{B}_s^0\rangle, \tag{15}$$

where the eigenvalues eare given by

$$\lambda_{L/H}^{(s)} = \left(M_0 - \frac{i}{2}\Gamma_0\right) \pm \left(M_{12} - \frac{i}{2}\Gamma_{12}\right)\frac{q}{p} = M_{L/H} - \frac{i}{2}\Gamma_{L/H}$$

and

$$f_\pm^{(s)}(t) = \frac{1}{2}\left[e^{-i\lambda_L^{(s)}t} \pm e^{-i\lambda_H^{(s)}t}\right]. \tag{16}$$

The flavour states of Eqs. (14) and (15) can either remain unchanged (+) or oscillate into each other (-).

The decay amplitudes are defined by

$$A_f = \langle f|H|B_s^0\rangle, \qquad A_{\bar{f}} = \langle \bar{f}|H|B_s^0\rangle,$$
$$\bar{A}_f = \langle f|H|\bar{B}_s^0\rangle, \qquad \bar{A}_{\bar{f}} = \langle \bar{f}|H|\bar{B}_s^0\rangle,$$

and transform also under CP. There are actually three different types of CP violation in B-decays:

1. CP violation in the decay amplitudes (also referred to as direct CP violation), which occurs in both charged and neutral decays, when the amplitude for a decay and its CP conjugate process have different magnitudes. In this case

$$|A_f| \neq \left|\bar{A}_f\right| \qquad \Longrightarrow \qquad \text{CP violation.}$$

2. CP violation in the mixing, which occurs when the two neutral mass eigenstates cannot be chosen to be CP eigenstates. When CP is conserved, the mass eigenstates are CP eigenstates. In this case the relative phase between M_{12} and Γ_{12} vanishes and the ratio $\frac{q}{p}$ given in Eq. (13) is equal to 1. Otherwise,

$$\left|\frac{q}{p}\right| \neq 1 \qquad \Longrightarrow \qquad \text{CP violation.}$$

3. CP violation in the interference between the decay anplitudes and mixing (so called mixing-induced CP violation), which occurs in decays into final states that are common to B_s^0 and $\bar{B}_s^0$.

$$\lambda_f = \frac{q}{p}\frac{\bar{A}_{f_{CP}}}{A_{f_{CP}}} \qquad \lambda_{\bar{f}} = \frac{p}{q}\frac{A_{\bar{f}_{CP}}}{\bar{A}_{\bar{f}_{CP}}}$$

$$\begin{aligned} \lambda_f\lambda_{\bar{f}} \neq 1 \longleftrightarrow \arg(\lambda_f) + \arg(\lambda_{\bar{f}}) \neq 0 \qquad &\Longrightarrow \qquad \text{CP violation} \\ \longrightarrow \text{if } f = \bar{f} \Rightarrow \mathrm{Im}(\lambda_f) \neq 0 \qquad &\Longrightarrow \qquad \text{CP violation.} \end{aligned}$$

The study of CP violation implies the measurement of the time-dependent decay asymmetry $\mathcal{A}_{\rm CP}^{obs}(t)$ between the $\bar{B}_s^0$ and the B_s^0

$$\mathcal{A}_{\rm CP}^{obs}(t) \equiv \frac{\mathcal{R}(\bar{B}_s^0(t) \to \bar{f}) - \mathcal{R}(B_s^0(t) \to f)}{\mathcal{R}(\bar{B}_s^0(t) \to \bar{f}) + \mathcal{R}(B_s^0(t) \to f)},$$

with t the proper time, $\mathcal{R}$ the observed decay rates and f the final state [4].

The decay rates can be calculated analytically with a possible mistag probability ω (see Section 2.4) as

$$\begin{aligned} \mathcal{R}_f(t) &= \mathcal{R}_{B_s^0\to f}(t) = |A_f(0)|^2\,\frac{e^{-\Gamma_s t}}{2}\left[\cosh\left(\frac{\Delta\Gamma_s\, t}{2}\right) + (1-2\omega)\,\cos(\Delta M_s\, t)\right]; \\ \bar{\mathcal{R}}_f(t) &= \mathcal{R}_{\bar{B}_s^0\to f}(t) = |A_f(0)|^2\,\frac{e^{-\Gamma_s t}}{2}\left[\cosh\left(\frac{\Delta\Gamma_s\, t}{2}\right) - (1-2\omega)\,\cos(\Delta M_s\, t)\right]. \end{aligned}$$

The observed flavour asymmetry $\mathcal{A}_f^{obs}$ can then be defined as

$$\mathcal{A}_f^{obs}(t) \quad = \quad D\mathcal{A}_f^{th}(t)$$

where the dilution factor D reduces to $D = (1 - 2\omega)$ in case of perfect resolution and the theoretical flavour asymmetry reads

$$\mathcal{A}_f^{th}(t) \equiv \frac{\bar{\mathcal{R}}_f(t) - \mathcal{R}_f(t)}{\bar{\mathcal{R}}_f(t) + \mathcal{R}_f(t)} = -\frac{\cos(\Delta M_s\ t)}{\cosh\left(\frac{\Delta\Gamma_s\ t}{2}\right)}. \tag{17}$$

1.2 The LHCb experiment at CERN

LHC is the Large Hadron Collider at CERN. Its 27 km circular tunnel will allow collisions of proton bunches with a center of mass energy of $\sqrt{s} = 14$ TeV. The LHCb experiment (Large Hadron Collider beauty experiment) is one of the four experiments that will take place at the LHC.

LHCb is a single-arm spectrometer (see Fig. 3 for the full layout of the detector) with a forward angular coverage from approximately 10 mrad to 300 (250) mrad in the bending (non-bending) plane. The choice of the detector geometry is motivated by the fact that at high energies both the b- and $\bar{b}$-hadrons are predominantly produced in the same forward (or backward) cone.

1.3 Motivations for this study

In 2002–2003, several studies had been performed on various decay channels to assess the physics performances of the LHCb experiment. References [5, 6] describe the study of the $B_s^0 \to D_s^-\pi^+$ and $B_s^0 \to D_s^\pm K^\mp$ decay channels. Since then, the generation, the simulation and the reconstruction software of the LHCb detector have evolved. The efficiencies and physics performances might have changed. This study proposes to redo the analyses with the new simulated data (Data Challenge '04, DC04) for the $B_s^0 \to D_s^-\pi^+$ decay.

2 The LHCb experiment

The LHCb experiment is described in this chapter. The first section gives a general layout of the detector. The following sections describe the trigger, particle identification and flavour tagging needed in the experiment. Finally the motivation for choosing the $B_s \to D_sH$ (both $B_s \to D_s^\mp K^\pm$ and $B_s \to D_s^-\pi^+$) decays is given.

2.1 The LHCb detector

The main features of the detector are described below (see also Fig. 3 for a full layout of the detector) [7–10].

The Beam Pipe: the protons bunches fly inside a beam pipe which is separated into three main parts. A 1.8 m long section around the interaction point has a

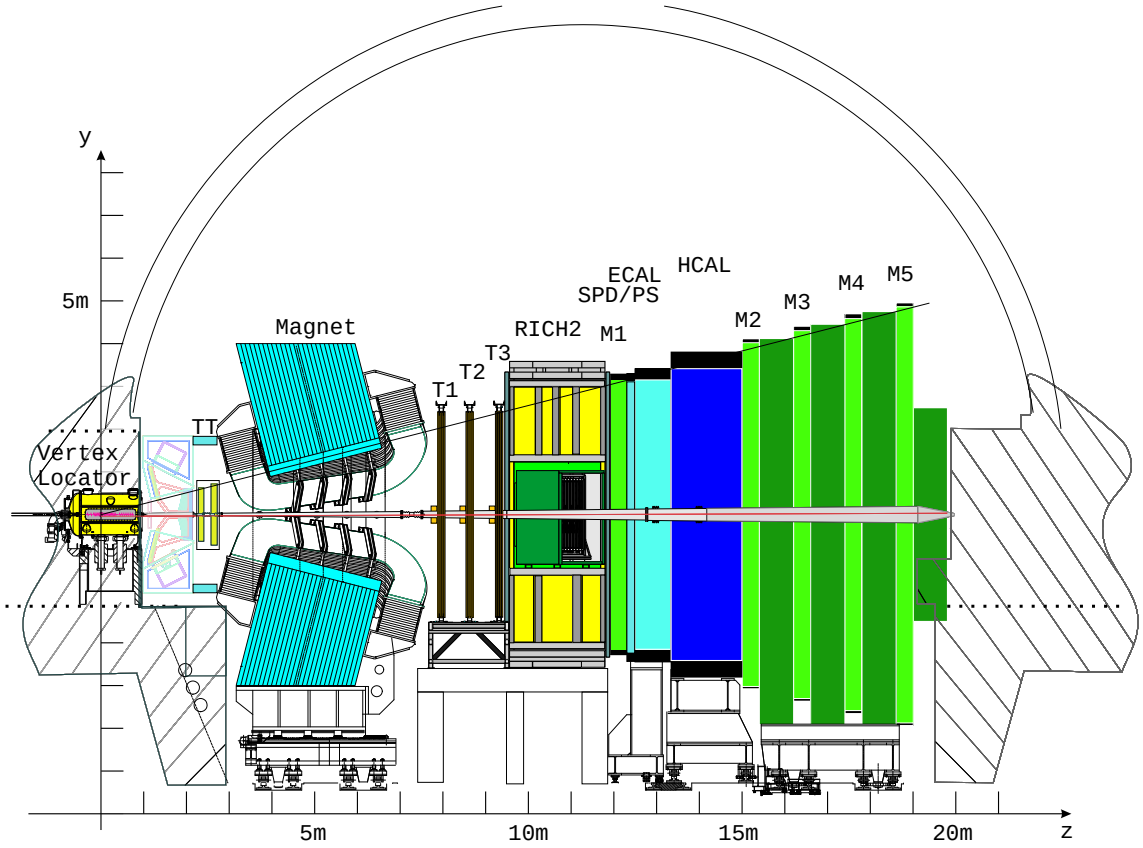

FIG. 3: Global layout of the LHCb detector (non bending plane).

large diameter of approximately 120 cm. This part is followed by two conical sections; the first is 1.4 m long with 25 mrad opening angle, and the second is 17.3 m long with 10 mrad opening angle.

The Vertex Locator (VeLo): vertex reconstruction is a fundamental requirement for the LHCb experiment. The presence of displaced secondary vertices (see Fig. 4) with respect to the primary vertex (pp interaction vertex) is a distinctive feature of b-hadron decays. The VeLo has to provide precise measurements of track coordinates close to the interaction region. These are used to reconstruct all the production and decay vertices, especially those of beauty- and charm-hadrons which are interested for LHCb, to provide an accurate measurement of their decay lifetimes, and to measure the impact parameter (IP, see definition on Fig. 4) of particles. The VeLo contains 21 silicon stations placed along the beam direction, for r and ϕ measurements.

The RICH (Ring Imaging CHerenkov) detectors: the RICH1 device is located between the VeLo and the TT (Trigger Tracker) tracking station (as seen on Fig. 3). The RICH2 detector is located between the third tracking station (T3) and the first muon chamber (M1). These detectors use the Cherenkov effect to identify particles. High momentum particles (up to $\sim$100 GeV/c) are identified by the RICH2 detector. Lower momentum particles, up to $\sim$60

GeV/c, are identified by the RICH1 detector. It combines silica aerogel and fluorocarbon gas radiators with a polar angle acceptance from 25 to 300 mrad. The pattern of hit pixels observed in the RICH photo-detectors is compared to the pattern that would be expected under a given set of mass hypotheses for the reconstructed tracks passing through the detectors, using the knowledge of the RICH optics. A likelihood (see chapter 2.3.1) is determined from this comparison and then the track mass-hypotheses are varied to maximise the likelihood. The RICH systems give as output a set of probabilities for each single particle type hypothesis, which are then combined to give a "best" identification of a charged track (see Section 2.3.1).

The Trigger Tracker (TT): this tracker is located downstream of RICH1 and in front of the LHCb magnet. It has a two-fold purpose. Firstly, it will be used in the L1 trigger (see chapter 2.2.2) to assign transverse-momentum information to large-impact parameter tracks. Secondly, it will be used in the offline analysis to reconstruct the trajectories of long-lived neutral particles that decay outside of the fiducial volume of the VeLo and of low-momentum particles that are bent out of the acceptance of the experiment before reaching tracking stations T1–T3 (see below).

The Magnet: the dipole magnet provides a vertical field with a good homogeneity across a 4.3 m horizontal aperture. The overall size is minimised by placing the magnet immediately downstream of RICH1, where it provides the 300 (horizontal) $\times$ 250 (vertical) mrad acceptance required for the downstream detectors. The central field is 1.1 T and together with a 4.3 by 3.6 m free aperture, it provides a corresponding bending power along the beam axis of 4.0 Tm. This field gives adequate momentum resolution with the proposed tracking system over the full acceptance.

T1–T3: these are the three tracking stations called T1, T2 and T3 placed immediately after the magnet. Each station consists of the Inner Tracker (IT) close to the beam pipe and the Outer Tracker (OT) surrounding the IT. The OT is made of straw tubes and the IT of silicon strip detectors. They are used to track charged particles.

The Calorimeters: there are actually three different parts for the calorimeters: the pad/preshower detector, the electromagnetic calorimeter and the hadronic calorimeter. The calorimeter system is used at several stages. It provides high transverse energy hadron, electron and photon candidates for the first trigger level. It provides the identification of electrons which is essential to flavour tagging through semileptonic decays.

The Muon Stations: muons are identified by extrapolating well reconstructed tracks with $p > 3$ GeV/c to the muon stations.

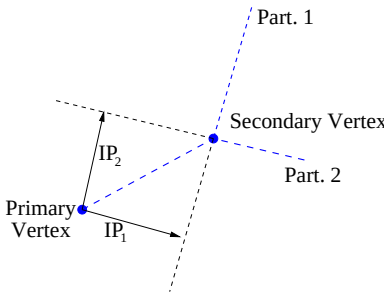

FIG. 4: Definition of the Impact Parameter (IP, unsigned).

2.2 The LHCb trigger

The LHCb experiment is designed to exploit the large number of $b\bar{b}$ pairs produced in proton-proton pp interactions at $\sqrt{s} = 14$ TeV at the LHC, in order to make precise studies of CP asymmetries and rare decays of b-hadrons. The LHCb experiment plans to operate at an average luminosity of $2 \times 10^{32}\text{cm}^{-2}\text{s}^{-1}$, i.e. much lower than the maximum design luminosity of the LHC in order to reduce the radiation damage. A further advantage is that at this luminosity the number of interactions per crossing is dominated by single interactions, which facilitates the triggering and reconstruction by ensuring low channel occupancy. Due to the LHC bunch structure and low luminosity the frequency of crossings with visible interactions by the spectrometer is about 10 MHz, which has to be reduced by the trigger to a few kHz, at which rate the events are written to storage for further offline analysis. This reduction is achieved in three trigger levels: Level-0 (L0), Level-1 (L1) and the High Level Trigger (HLT). L0 is implemented in custom electronics, while L1 and the HLT are executed on a farm of commodity processors.

2.2.1 Level-0 trigger

The L0 trigger has an input rate of 40 MHz and an output rate of 1 MHz. It is based on the identification of leptons, hadrons and photons with high-transverse momentum (p_T) in calorimeters (scintillating pad detector, preshower, electromagnetic and hadronic calorimeters) and muon chambers, combined with a pile-up veto. The pile-up veto unit identifies bunch crossings with more than one pp interaction using a dedicated part of the vertex detector system and the calorimeters [11].

The L0 decision unit decides whether an event is kept for the next level. About 90% of the output rate is given to events with a single high-p_T muon, electron or hadron. The p_T thresholds can be adjusted according to physics needs. At present it is assumed that events with high-p_T muon, electron and hadron share 20%, 10% and 60% of the total trigger rate, respectively. The remaining 10% of the output rate is reserved for events with a single high-p_T photon, multi-leptons and some other combinations. In the case of a positive decision, the L0 decision unit passes the information on the high-p_T particle to the L1 trigger tracker to be used as a seed in the tracking algorithm. The same information is also given to the L1 decision unit. The L0 decision unit is programmable so that the selection criteria can be

easily changed to reflect physics interests.

2.2.2 Level-1 trigger

The L1 trigger has an input rate of 1 MHz and an output rate of 40 kHz. This level is required to be fast, efficient, flexible and robust. It will select all the interesting b-decays with some additional bandwidth for systematic studies [11–14].

This level will have access to the data from the VeLo and TT tracking stations as well as all the L0 objects. The strategy used is to reconstruct all the VeLo tracks in 2D, select those in a defined IP window, then reconstruct the 3D tracks and apply a tighter IP window selection. The momentum of each selected track is also measured using the fringe field in front of the magnet (VeLo-TT matching), which gives a momentum resolution of $\sim 20 - 40\%$.

L1 will actually use different streams for the selection of events with some overlap. These lines are:

$p_{T,1}$, $p_{T,2}$: the charged tracks with highest p_T in the event are selected and their p_T are tested.

Dimuons: if pairs of muons are found in the event, their mass and IP are tested.

J/ψ: the algorithm will also look for dimuons coming from J/ψ (which decays in $\mu\mu$ in 5.88% of the cases) and test their reconstructed mass.

Single-muon: the p_T and IP of single muons are also tested.

Photons: the highest transverse energy of all the photons found in the event is tested.

Electrons: finally the transverse energy and p_T of the electrons found in the event are also tested.

The cuts for these different lines are shown in the Appendix A.

2.2.3 High Level Trigger

The HLT will have an input of 40 kHz (output of L1) and is designed to have an output rate of 200 Hz of exclusive events plus 1.8 kHz of other events as given below [12–14].

1. 200 Hz of specific B-decays, primordial for LHCb physics goals or used as control channels (e.g. for tagging).

2. 600 Hz of high mass dimuons, used for the calibration of the tracking and to study the lifetime of unbiased $b \to J/\psi X$ events to obtain information about the decay time resolution.

3. 300 Hz of D^*, used for the calibration of the hadron PID (Particle IDentification) and for the study of CP violation in charm decays.

4. 900 Hz of inclusive-b (e.g. $b \to \mu$), used for the calibration of the trigger, for the study of the lifetime bias due to the trigger and for the study of B physics (data mining).

This level of trigger uses all data from the detector to enhance the b content and identify events with μ and J/ψ (generic HLT) and to select specific b decays (specific HLT). The generic HLT will first reduce the rate down to 10–15 kHz. The strategy used here is to reconstruct all the tracks in 3D and select a collection of tracks candidates in a defined IP window, followed by a full long tracking (VeLo $\rightarrow$ TT $\rightarrow$ T1–T3). L1 is then redone with a better momentum measurement using T1-T3 (which gives $\sigma_p/p < 6\%$).

The specific HLT will be run after the generic HLT. A specific set of cuts is defined for each decay channel, including sidebands.

This study will not use the HLT algorithms as these are not fully implemented yet. At the time of the TDR, the HLT efficiency had not been studied yet, and was assumed to be 100% for simplicity. This efficiency is currently estimated to be $\sim$85% for the $B_s^0 \to D_s^- \pi^+$ channel. The total efficiencies and yields given in Section 5.1 will have to be scaled down by this factor as soon as it will be known more precisely.

2.3 Particle identification

For both event selection and flavour tagging (see chapter 2.4), a good particle identification (PID) is of high importance. This is provided by the calorimeter systems, muon chambers and the RICH detectors, which has been described in Section 2.1. Section 2.3.1 explains how this PID information is used in the offline selection, through a DLL function (Delta Log Likelihood).

2.3.1 Delta Log Likelihood

The selection of tracks according to their PID is based on a DLL hypothesis which combines the information from various subdetectors to assign a PID. The function is of the type

$$\text{DLL(A-B)} \equiv \Delta \ln \mathcal{L}_{AB} = ln\left[\mathcal{L}(A)/\mathcal{L}(B)\right] \tag{18}$$

where the two likelihood functions are a composition of information from all different parts of the detector. For example

$$\begin{aligned}
\mathcal{L}(e) &= \mathcal{L}^{RICH}(e)\mathcal{L}^{CALO}(e)\mathcal{L}^{MUON}(non\ \mu) \\
\mathcal{L}(\mu) &= \mathcal{L}^{RICH}(\mu)\mathcal{L}^{CALO}(non\ e)\mathcal{L}^{MUON}(\mu) \\
\mathcal{L}(h) &= \mathcal{L}^{RICH}(h)\mathcal{L}^{CALO}(non\ e)\mathcal{L}^{MUON}(\mu)
\end{aligned}$$

where h stands for hadron, e for electron, μ for muon and each of these new functions compute the probability for the given type of particle. If there are more than one estimator from a given detector, they can be simply combined by taking the product of their individuals likelihoods.

The function (18) tends to have positive values for correctly A-type identified particles and negative for correctly B-type identified particles.

2.4 Flavour tagging at LHCb

The knowledge of the initial flavour of the reconstructed B mesons is necessary in order to study the time dependent CP and flavour asymmetries [15].

The statistical uncertainty on the measured CP asymmetry is directly related to the effective tagging efficiency ϵ_{eff}:

$$\sigma^2_{\mathcal{A}} = \frac{1-\mathcal{A}^2_{\rm obs}}{N_{\rm phys}\epsilon_{\rm tag}(1-2\omega)^2} = \frac{1-\mathcal{A}^2_{\rm obs}}{N_{\rm phys}\epsilon_{\rm eff}} \propto \frac{1}{\epsilon_{\rm eff}},$$

where

$$\epsilon_{\rm eff} = \epsilon_{\rm tag} D^2 = \epsilon_{\rm tag}(1-2\omega)^2,$$

$\epsilon_{\rm tag}$ is the tagging efficiency (probability that the tagging procedure gives an answer), ω is the wrong tag fraction (probability for the answer to be incorrect when a tag is present), D is the dilution term and $N_{\rm phys}$ is the number of selected and triggered events. The probabilities $\epsilon_{\rm tag}$ and ω are calculated as

$$\epsilon_{\rm tag} = \frac{R+W}{R+W+U} \qquad\qquad \omega = \frac{W}{R+W},$$

where R, W, U are the number of correctly tagged, incorrectly tagged, and untagged events, respectively. Thus $\epsilon_{\rm eff}$ needs to be maximised in order to minimise $\sigma_{\mathcal{A}}$.

There are basically two different ways for tagging an event:

- opposite-side tag (e, μ, K, secondary vertex charge),

- same-side tag (K for B_s, π for B_d).

Opposite-side tag algorithms aim at determining the flavour of the b hadron accompanying the signal B meson. They use the charge of the lepton from semileptonic b decay and of the kaon from $b \to c \to s$ decay chain. They also use the charge of the inclusive secondary vertex reconstructed from the opposite side b-decay products. When the accompanying b hadron is a neutral B meson, due to the possibility of flavour oscillations, all these methods have an intrinsic dilution.

Same side tags determine directly the flavour of the signal B meson exploiting the correlation in the fragmentation decay chain. If a B^0_s ($\bar{b}s$) is produced in the fragmentation of a $\bar{b}$ quark, an extra $\bar{s}$ is available to form a K meson. When the meson of interest is a B^0_d instead of a B^0_s, the algorithms will look for a same side π instead of a K.

2.5 The $B_s^0 \to D_s H$ decays

The $B_s^0 \to D_s^- \pi^+$ and $B_s^0 \to D_s^\pm K^\mp$ decays have the same topology, illustrated in Fig. 5. Since both the B_s^0 and the $D_s^\pm$ fly (lifetimes of respectively 1.5 and 0.5 ps), two detached vertices will be visible in the event. This fact will be used for the selection of these decays. The $D_s^\pm$ will be required to decay to $K^+K^-\pi^\pm$ because this decay has a significant branching ratio. This decay actually includes several resonances (e.g. $\phi \to K^+K^-$, $K^{*0} \to K\pi$) whose mass could be used as a selection criteria. The branching ratios (BR) are given in Table 1 and the relative fraction of the different resonances assumed in EvtGen are given in Table 2. The selection will actually skip the resonances and hence all decays with $KK\pi$ final states can be selected.

Tab. 1: Relevant $B_s^0 \to (D_s^- \to K^+K^-\pi^-)\pi^+$ branching ratios. Measured values are found in [22].

Decay	BR	estimated as
$B_s^0 \to D_s^-\pi^+$	$(2.76\pm0.25) \times 10^{-3}$	$B^0 \to D^-\pi^+$
$D_s^- \Rightarrow K^+K^-\pi^-$	$(4.4\pm1.2) \times 10^{-2}$	measured
Visible $B_s^0 \to (D_s^- \to K^+K^-\pi^-)\pi^+$		$(121\pm35) \times 10^{-6}$

Tab. 2: Relative fraction of the different resonances of $D_s^- \Rightarrow K^+K^-\pi^-$ assumed in EvtGen, taken from [22].

Decay	Fraction
$D_s^- \to (\phi \to K^+K^-)\pi^-$	36.36%
$D_s^- \to (\bar{K}^{*0} \to K^+\pi^-K^-$	45.16%
$D_s^- \to K^+K^-\pi^-$	18.48%

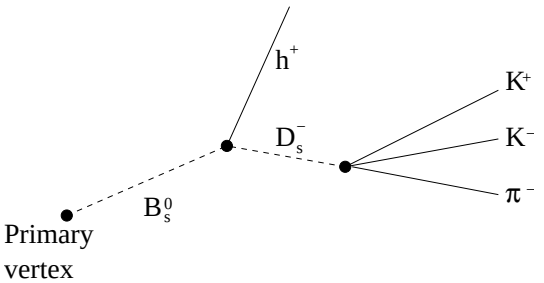

Fig. 5: Topology of a $B_s^0 \to D_s^- H^+$ decay.

The $B_s^0 \to D_s^-\pi^+$ decay is flavour specific in which a single tree diagram contributes. Flavour specific means that B_s^0 decays instantaneously as $D_s^-\pi^+$ and $\bar{B}_s^0$ instantaneously as $D_s^+\pi^-$. Moreover, no CP-violation is expected in this channel.

Looking back at Eq. (17), it appears that the motivations for studying the $B_s^0 \to D_s^- \pi^+$ decay channel are the extraction of the parameters ΔM_s, $\Delta\Gamma_s$ as well as determining the wrong tag fraction ω. These parameters can then be used with other results to get the phases defined in Section 1.1.

For example, the decay $B_s^0 \to D_s^\pm K^\mp$ gives access to $\phi_s + \gamma$ but the knowledge of ΔM_s and $\Delta\Gamma_s$ is needed for the extraction of $\phi_s + \gamma$. Also the wrong tag fraction is needed. As $B_s^0 \to D_s^- \pi^+$ and $B_s^0 \to D_s^\pm K^\mp$ have the same topology, it can be assumed that the wrong tag fraction is the same for both decay. Thus using the fact that $B_s^0 \to D_s^- \pi^+$ is flavour specific, it can be used as a control channel for $B_s^0 \to D_s^\pm K^\mp$. Finally using e.g. the $B_s^0 \to J/\psi\ \phi$ decay to get ϕ_s and combining all this information together leads to γ.

3 Software and data

3.1 Software and simulation

The Monte Carlo study of the LHCb experiment uses a hierarchy of programs to generate the events, simulate the interaction between the generated particles and the detector, reconstruct these particles from the output of the simulated detector and analyse these reconstructed particles. All these programs are based on the Gaudi framework (which is C++ based) except for Pythia which is written in Fortran. Here is the hierarchy:

General Framework:

- Gaudi
  - Generation / Simulation:
    - Gauss
      i. Pythia
      ii. Geant4
      iii. EvtGen
  - Digitization:
    - Boole
  - Reconstruction:
    - Brunel
  - Analysis:
    - DaVinci–LoKi

Here is a short description of the main features and roles of each of these software packages (for more information, see [16–19]):

Gauss deals with the generation and the simulation of all types of events. It is composed of the three following softwares.

PYTHIA is used to generate high-energy physics events, i.e. sets of outgoing particles produced in the interactions between two incoming particles. The emphasis is on multi-particle production in collisions between elementary particles, in particular hard interactions in pp colliders (as LHC). The program is based on a combination of analytical results and various QCD-based models. This program does the physics event generation, where minimum-bias pp interactions at $\sqrt{s} = 14$ TeV are generated.

EVTGEN is an event generator designed for the simulation of the physics of B decays. In particular, EVTGEN provides a framework to handle complex sequencial decays and CP violating decays.

GEANT4 is a toolkit for the simulation of the passage of particles through matter. It is this program that simulates the interaction between all the particles and the detector.

BRUNEL is the LHCb reconstruction program. At this stage the simulated tracks are reconstructed from hits in all parts of the detector.

BOOLE is the LHCb digitization program. It reads in the output of the detector simulation (GAUSS), adds hits from spillover events and LHC background, and simulates the detector response. The output is digitized data that mimics the data coming from the real detector.

DAVINCI is the offline analysis software. This program is used to perform the selection of particles and the gathering of all the data needed to perform the event selection. This package along with LOKI (see below) gives access to informations both about Monte Carlo (MC) truth and reconstructed events.

LOKI is a package for a simple and user-friendly data analysis, embedded in DaVinci. The current functionality of LOKI includes the selection of particles, manipulation with predefined kinematics expressions, loops over combinations of selected particles, creation of composite particles from various combinations of particles, flexible manipulation with various kinematics constraints, creation of n-tuples and access to Monte Carlo truth information.

The n-tuples created with DAVINCI-LOKI will then be read and analysed with Root [20] which is an object-oriented framework aiming at solving the data analysis challenges of high-energy physics.

The main selection code will be written in C++ within DAVINCI using some of the LOKI features.

3.2 The Monte Carlo data

All simulated data is stored at CERN on a dedicated server in the form of DST files of 500 events each. These files can easily be read with DAVINCI for analysis.

The event selection aims at achieving the highest efficiency on signal events while rejecting the background originating from random combinations or other b decays.

The pure combinatorial background can lead to a B_s meson candidate and can occur in any interaction, such as minimum-bias (Section 3.2.3). However since the signature of b events is the presence of detached secondary vertices, it is assumed that the dominant source of background is that arising from events with a $b\bar{b}$ pair (so called inclusive-$b\bar{b}$ sample, see Section 3.2.4).

The first subsection of this section will discuss some general considerations, while in the following subsections the data is actually described in more details,

3.2.1 Random number generation for the MC events

To generate the MC data, a random number (seed) is generated as a 32 bit number. But it has been found that one of the functions used later in the generation chain was actually using only the 24 least significant bits. It then means that the seed was randomly chosen out of "only" 2^{24} (= 16'777'216) instead of the 2^{32} (= 4'294'967'296) first thought. If two events have the same seed, they will be identical. The consequence is that in a generation of 60 M events (which is what has been obtained for the inclusive-$b\bar{b}$ event sample), only ∼17 M events are actually independent (at most, i.e. if all seeds are used at least once). This is true in any sample of generated events. A correction factor must then be applied to the number of events counted in each subset of the initial sample. The number of independent events equals [21]:

$$N_{\text{indep}} = M - M\left(1 - \frac{1}{M}\right)^N \approx M\left(1 - e^{-\frac{N}{M}}\right) \tag{19}$$

$$\begin{aligned}\sigma^2_{N_{indep}} &= M(M-1)\left(1-\frac{2}{M}\right)^N + M\left(1-\frac{1}{M}\right)^N - M^2\left(1-\frac{1}{M}\right)^{2N} \\ &\approx N_{\text{indep}} \cdot e^{-\frac{N}{M}}\end{aligned} \tag{20}$$

where $M = 2^{24}$ and N is the number of events of the original sample. The fraction of independent events in a sample of generated inclusive-$b\bar{b}$ events is then

$$f_{\text{indep}} = \frac{N_{\text{indep}}}{N} \tag{21}$$

The assumption that will be made in this study is that this fraction of independent events is the same in all subsets of the initial sample. The main consequence of this assumption is that the event selection efficiencies will remain the same but not the binomial errors on these efficiencies (see Section 5.1.1 for more details).

3.2.2 $B_s^0 \to D_s^- \pi^+$ events

This study is performed on $B_s^0 \to D_s^- \pi^+$ events (including charge conjugates, cc) generated at CERN using Gauss v15r7 and v15r11, Boole v5r8 and v5r9 and Brunel v23r7. A total amount of nearly 4M events was analysed using DaVinci v12r5 and LoKi v3r6. This data can be found on the LHCb bookkeeping site [2].

[2] [http://lhcbdata.home.cern.ch/lhcbdata/bkk/]

Each event on these tapes contains the signal of interest where the B_s is forced to decay to $D_s^-\pi^+$ (and cc) and where the $D_s^- \Rightarrow K^+K^-\pi^-$ decay includes resonances (Section 2.5). The efficiency of reconstruction or selection in the sample are far from 100% because for example some B_s decay products fall outside the geometric acceptance. The analysis for this type of events can be found in Sections 4.3 and 5.1.

3.2.3 Minimum-bias data

The second type of data that has been analysed is called Minimum-bias events. Minimum-bias means that the events found in these data have been generated and simulated with no bias, no constraint on what decay to find in the event. They are unbiased pp events. The same softwares as for the inclusive-$b\bar{b}$ data have been used for the analysis of this data. The data that was used had already been stripped requiring both positive L0 and L1 decisions. Note that this data is analysed as a check of the selection algorithm. Actually, since displaced vertices are required, this background should not be dangerous. Thus, given the small sample analyzed (12M events correspond to about 1 second of LHCb), no event should pass the selection cuts.

The results found for this part are presented in Section 4.3.2.

3.2.4 Inclusive-$b\bar{b}$ data

The tuning of the cuts will be performed first on a sample of ∼2M inclusive-$b\bar{b}$ events. These inclusive-$b\bar{b}$ data have been generated with the constraint that at least one b or $\bar{b}$ hadron is in the 400 mrad angular acceptance. Thus all the possible decays of b-hadrons can be found in this data in the proportions of their respective visible branching ratios (which include the fraction of b's going to each particular b-hadron, the branching ratio of the decay and of the sub-decay). This so-called tuning will actually not be performed on an event-per-event basis [3] (see Section 4.2) which means that the results found for this first sample will not be biased. This will still be verified on a second sample of ∼2M. Then another ∼16M events sample will be added, leading to a total of 20.5M events analyzed.

The result of this study will be reported in Sections 4.3.3 and 5.1.

3.2.5 Specific background data

After the analysis of the inclusive-$b\bar{b}$ sample, some specific background will be found in the selected events. These decays will be further studied by analysing some specific background data. The decays of interest that will be found in the background are:

- $B_d^0 \to D^-\pi^+$
- $\Lambda_b \to \Lambda_c^+\pi^-$

[3] The event-per-event basis means to adjust the cuts to remove some particular selected events.

Other types could appear with more statistics. Only the first decay has been generated and is accessible through the LHCb bookkeeping site. The results for the analysis of 110k events of the $B_d^0 \to D^-\pi^+$ can be found in Section 4.3.4. Some other specific background will be found in the selected inclusive-$b\bar{b}$ events. It will be explained in Section 4.3.3 why these other decays haven't been studied in more details.

4 Selection of events

Before any fine tuning of the cuts is performed, all candidates of the decay of interest must be selected using loose cuts. In the $B_s^0 \to (D_s^- \to K^+K^-\pi^-)\pi^+$ decay, four tracks combinations are looked for to create first the D_s from 3 tracks and then the B_s using the bachelor pion and the reconstructed D_s. Thus the first step in the selection code is to loop over all pions and kaons found in the event and look for possible combinations that would make D_s and B_s candidates. Then these candidates will have to pass a set of predefined cuts to select only the best candidates for signal events. These cuts are presented in the following few sections. In Section 4.1, the preselection cuts are defined. These cuts will reduce both the signal and background samples. A Root analysis will then be used to study the remaining data and to tune the cuts so that the efficiency of the signal selection and the background rejection factor are both as high as possible. This is presented in Section 4.2. Finally in Section 4.3, the results of the selection using the tuned final cuts are shown.

During the selection, several candidates per event are allowed; note that the numbers shown in this study are numbers of events and not numbers of candidates.

4.1 Preselection of signal and $b\bar{b}$ events

First a sample of ∼2 M events of inclusive-$b\bar{b}$ background events and ∼4 M events of signal were analysed at a preselection level to tune the cuts. The main analysis code included a set of cuts for preselection and another set for final selection. These two sets had been optimised on the TDR data. They had to be changed to better suit the new DC04 data. Below is a presentation of the new selection cuts that have been used to preselect all data needed for this study. The code that has been used is an updated version of PhysSel/Bs2DsH v3r3p1.

The selection only looks at decays that are constructed from long tracks, i.e. with the four tracks leaving some clusters in the VeLo and in the T1–T3 stations.

The selection is actually separated into three distinct parts: selection of the tracks, selection of the D_s using three tracks and selection of the B_s using the selected D_s and the fourth track.

1) Preselection of the tracks:

The selection of the four tracks is non-exclusive, which means that tracks can be

selected as more than one particle type. The identification of the tracks is achieved using loose cuts on the DLL difference between kaon and pion hypotheses and between kaon and proton hypotheses. The cuts have been set to: $\mathrm{DLL}(K-\pi) > -10$ and $\mathrm{DLL}(K-p) > -10$ for the kaons, $\mathrm{DLL}(\pi-K) > -10$ for the pions and are applied to all the tracks.

The particles originating from a B-meson decay have a transverse high momentum. All four final tracks are then required to have $p_T > 200$ MeV/c. Also, tu ssure well reconstructed tracks, a cut is set to P > 2 GeV/c.

It is possible to calculate the distance of closest approach between a track and a primary vertex, the so-called IP (unsigned, see Fig. 4). Using the errors on both the primary vertex (PV) position and the tracks parameters (x, y and z), an error on this IP can be estimated. The IP Significance (IPS) is then defined as

$$\mathrm{IPS} = \frac{\mathrm{IP}}{\sigma_{\mathrm{IP}}}. \tag{22}$$

In this study, multiple interactions are considered. Several primary vertices can be reconstructed in one event. The IP are then calculated with respect to all primary vertices. The PV from which the B_s originates is the vertex with respect to which the reconstructed B_s has the smallest IPS.

The particles originating from the decay of the D_s as well as the bachelor pion directions should not point back to the PV. They will then have a significant IP. For the preselection only the bachelor is required to have IPS > 1.

2) Preselection of the D_s^-:

The D_s is required to have a significant IP: IPS > 1 with respect to all PVs.

The mass of the reconstructed D_s should be close to the true mass, therefore it is required that the reconstructed mass falls within a ± 50 MeV/c^2 window around the true D_s mass [4] (i.e. $|M_{D_s,\mathrm{reco}} - M_{D_s,\mathrm{true}}| < 50$ MeV/c^2).

A vertex can be reconstructed using the tracks chosen to form the D_s. This vertex fit leads to a χ^2 which is small if the vertex is precisely defined. For the D_s vertex, it is required that $\chi^2 < 20$.

3) Preselection of the B_s^0:

The B_s is supposed to point back to the PV. Thus its IPS is supposed to be low and the selection requires that IPS < 20.

As for the D_s, the mass of the reconstructed B_s should be close to the true mass [5]. The requirement is here that the reconstructed mass falls within a ± 500 MeV/c^2 window around the true B_s mass (i.e. $|M_{B_s,\mathrm{reco}} - M_{B_s,\mathrm{true}}| < 500$ MeV/c^2). This cut is loose to artificially increase the background statistics.

For the B_s vertex, it is required that $\chi^2 < 10$.

[4] $M_{D_s,\mathrm{true}} = 1968.5$ MeV/c^2 in the generation, but the PDG value is $M_{D_s} = 1968.3$ MeV/c^2.

[5] The "true" mass of the B_s is the mass used for the generation: $M_{B_s} = 5369.6$ MeV/c^2 which in this case corresponds to the mass found in the PDG [22].

Due to the large boost in this experiment, the B_s will have a large momentum in the z direction (z being parallel to the beam axis) and will fly for a while before decaying to their final states. This leads to the requirement that the flight distance of the B_s should be significant, i.e. $\mathrm{FS}_{B_s} > 0$ for preselection, where

$$\mathrm{FS} = \frac{\|\overrightarrow{\text{Decay Vertex}} - \overrightarrow{\text{Origin Vertex}}\|}{\sqrt{\sigma^2_{\text{end}} + \sigma^2_{\text{origin}}}}. \tag{23}$$

As discussed before, the B_s should have its momentum pointing back to the primary vertex. This fact is further exploited by defining the angle θ_P between the vector from the B_s origin vertex and its decay vertex ($\vec{r}$) and the particle's momentum ($\vec{p}$). The definition is then

$$\cos(\theta_P) = \frac{\vec{p} \cdot \vec{r}}{|\vec{p}\,||\vec{r}\,|} \tag{24}$$

This cosine should be close to 1 (i.e. $\theta_P \sim 0$). The requirement on this parameter has been set to $\cos(\theta_P) > 0.9995$ for preselection.

Also, due to the large boost in the forward direction, the D_s is supposed to be found downstream of the B_s. So it is required that $z_{D_s} - z_{B_s} > 0$.

4) Cuts removed between the TDR study and the DC04 study:

Some of the cuts that were used at the time of the TDR were dropped for this study. Here is a short explanation for these six cuts dropped:

χ^2/DoF: the four tracks were asked to be fitted precisely from the track's reconstruction. The parameter showing the goodness of the fit is the χ^2 per degree of freedom. For each track it was asked that $\chi^2/DoF < 4$. This cut has been found to be rather inefficient for the rejection of $b\bar{b}$ events as ∼98% of the tracks that remain after all the other preselection cuts have $\chi^2/DoF < 4$. This χ^2 has changed between the two generations of data because the tracking and reconstruction algorithms have changed.

$\chi^2_{\text{Constr. Vtx}_{D_s}}$: when a mass constraint is asked, the parameters of the studied particle will be adjusted to get the correct mass. This adjustment of the parameters can induce a bias, for example on the proper time, which is not wanted. This cut was removed for this reason.

$\mathrm{FS}_{D_s-\mathrm{PV}}$: the distance significance from the primary vertex to the D_s decay vertex is obviously highly correlated to the distance significance between the primary vertex and the B_s. It was decided that the effect of only one flight distance with respect to the primary vertex would be taken into account: $\mathrm{FS}_{B_s-\mathrm{PV}}$.

$z_{B_s} - z_{\mathrm{PV}}$: again, the two cuts on Δz are highly correlated. It was decided to cut on the flight distance of the D_s.

$\mathrm{DLL}_K(K-e)$: this cut was not useful for this selection after all the other cuts had been applied.

All the cuts presented in this chapter, including the cuts of the analysis on the TDR data are summarized in Table 3. The number that changed between the two sets of cuts are written in bold.

TAB. 3: Preselection cuts on TDR and DC04 data. Changes between the two versions are written in bold font.

	TDR Preselection		DC04 Preselection	
Parameter	Min cut	Max cut	Min cut	Max cut
χ^2/NDF	—	4	—	—
P_H [GeV/c]	2	—	2	—
$P_{D_s\text{Prod}}$ [GeV/c]	2	—	2	—
$p_{T,H}$ [MeV/c]	200	—	200	—
$p_{T,D_s\text{Prod}}$ [MeV/c]	200	—	200	—
M_{B_s} [MeV/c^2] (l) [6]	4869.6	5869.6	4869.6	5869.6
M_{B_s} [MeV/c^2] (t) [7]	4869.6	5869.6	4869.6	5869.6
M_{D_s} [MeV/c^2]	1918.5	2018.5	1918.5	2018.5
IPS_{B_s}	—	20	—	20
IPS_{D_s}	1	—	1	—
IPS_H	1	—	1	—
$\text{IPS}_{D_s\text{Prod}}$	0	—	0	—
$\chi^2_{\text{Vertex}_{B_s}}$	—	10	—	10
$\chi^2_{\text{Vertex}_{D_s}}$	—	20	—	20
$\chi^2_{\text{Constr. Vtx}_{D_s}}$	—	10^{20}	—	—
$\text{FS}_{D_s-\text{PV}}$	0	—	—	—
$\text{FS}_{B_s-\text{PV}}$	—	—	**0**	—
$z_{B_s} - z_{\text{PV}}$ [mm]	0	—	—	—
$z_{D_s} - z_{B_s}$ [mm]	0	—	0	—
$\cos(\theta_P)$	0.9995	—	0.9995	—
$\text{DLL}_H(\pi - K)$	-5	—	**-10**	—
$\text{DLL}_\pi(\pi - K)$	-5	—	**-10**	—
$\text{DLL}_K(K - \pi)$	-5	—	**-10**	—
$\text{DLL}_K(K - p)$	-5	—	**-10**	—
$\text{DLL}_K(K - e)$	-5	—	—	—

4.2 Tuning of cuts

Once all data has been obtained using the preselection cuts, a tighter set of cuts must be found to get a background-over-signal ratio as low as possible and a selection efficiency as high as possible. This is done by tuning the preselection cuts defined in Section 4.1. What was done was actually not really a so-called tuning on an event-by-event basis: the tuning was done by studying the distributions of the relevant parameters both for the signal and the background selected candidates. A way of checking whether the selection has been biased or not is to re-run the selection on another sample of events. Another ∼2M events sample has been analysed and it was found that the efficiency of selection of the signal and of rejection of the background was the same for both samples. It was then decided to keep both samples to get as much statistics as possible.

The distribution for each of the preselection cuts is shown below for both the signal and the background events. The position of the tuned cut for the final selection is also indicated. All the distributions have been normalised to 1 by dividing the surface of the histogram by its integral.

1) Selection of the daughters of the D_s:

The p_T of the D_s products is plotted in Fig. 6 (a) to (c). The cut is such that $p_T > 300$ MeV/c. The plot shows that these cuts remove the first bin, which is where the level of background is the highest.

The IPS of the three daughters of the D_s are also used to reject some background with a cut at IPS > 3. The distributions of interest are shown in Fig. 6 (d) to (f).

Figure 7 (a) and (b) show the distributions of $\mathrm{DLL}_K(K-\pi)$. It is visible that the misidentification between kaons and pions can introduce a lot of background in the sample (for example the decay $B_d^0 \to (D^\pm \to K\pi\pi)\pi^\mp$). The cut on the identification is hence tightened to $\mathrm{DLL}_K(K-\pi) > -5$ as shown on the plot. The other cuts on the tracks identification were not considered as important. Moreover, keeping the cuts as loose as possible might increase the level of background but it also increases the total selection efficiency for the signal and hence the annual signal yield increases too.

2) Selection of the D_s^- and the bachelor:

The distributions of the p_T of the reconstructed D_s and of the bachelor π are shown in Fig. 8 (a) and (c). The D_s and bachelors are required to have their $p_T > 2000$ MeV/c and $p_T > 600$ MeV/c respectively. The cut for the D_s is easily justified graphically.

Figure 8 (b) and (d) show the distributions of the IPS of the D_s and the bachelor pion. These cuts are not tight but help removing a big part of the background.

The precision required for the fit of the D_s vertex is increased at this level of selection. The cut on the χ^2 is set to $\chi^2 < 16$. The distribution is plotted in Fig. 8 (e).

The cut on the mass of the D_s is one of the most efficient (see Fig. 8 (f)). It is tightened here to $|M_{D_s,\mathrm{reco}} - M_{D_s,\mathrm{true}}| < 15$ MeV/c^2 (which corresponds to a window of $\pm 3\sigma$; this result will be discussed in Section 5.3.1).

3) Selection of the B_s^0:

Figure 9 (a) shows the distributions of the IPS of the B_s. The cut on the B_s at IPS < 4 is tight because the B_s should point back to the primary vertex.

The χ^2 of the B_s decay vertex is required to be smaller than 9. The vertex of the B_s is supposed to be better defined than that of the D_s because the daughters have a bigger opening angle than those of the D_s. The distribution is plotted in Fig. 9 (b).

In a $B_s^0 \to D_s^-\pi^+$ event at LHCb, the B_s will fly a few cm. The cut on the

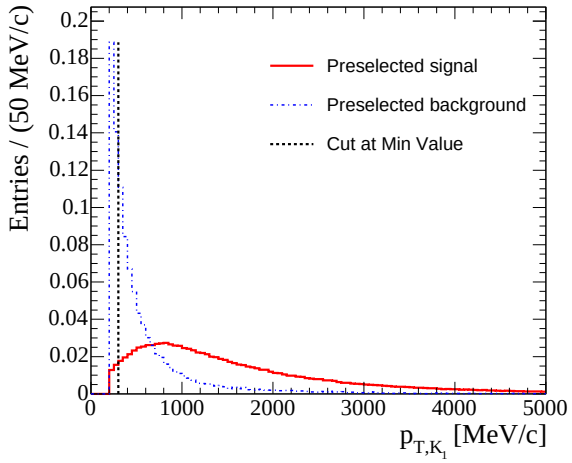

(a) p_T of the 1^{st} K

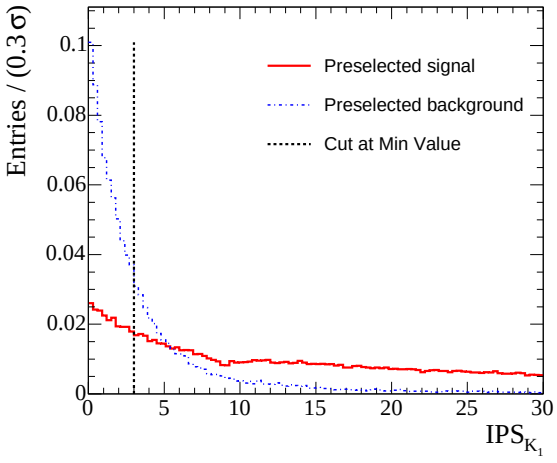

(d) IPS of the 1^{st} K

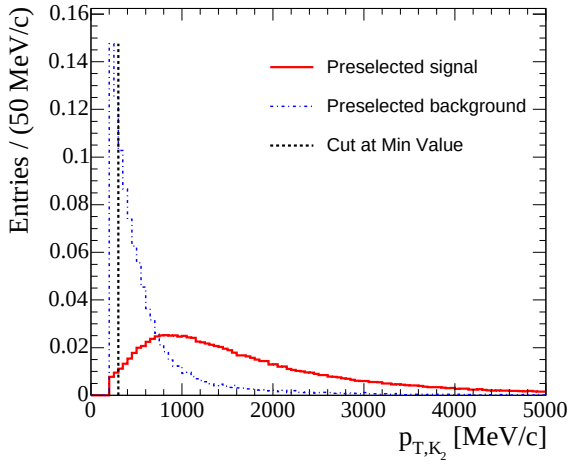

(b) p_T of the 2^{nd} K

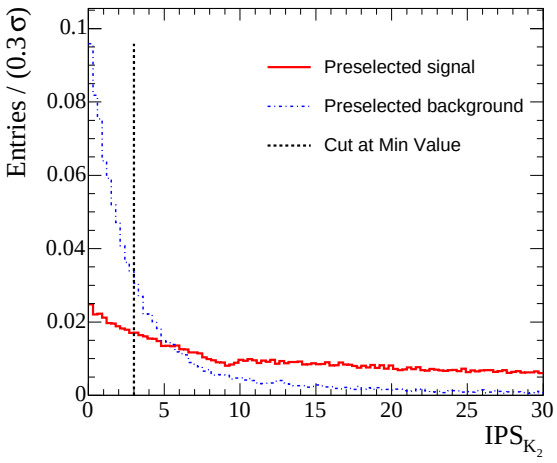

(e) IPS of the 2^{nd} K

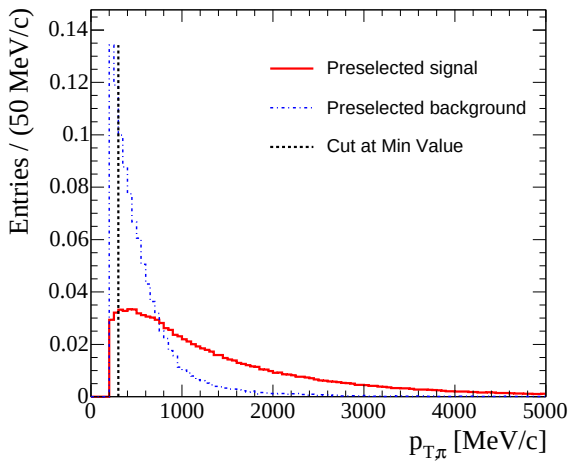

(c) p_T of the π

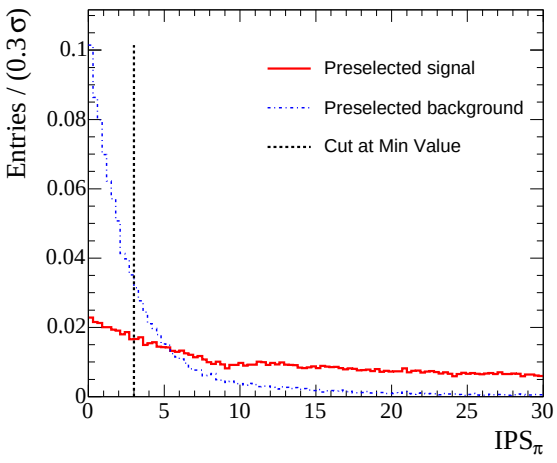

(f) IPS of the π

FIG. 6: D_s daughters p_T and IPS.

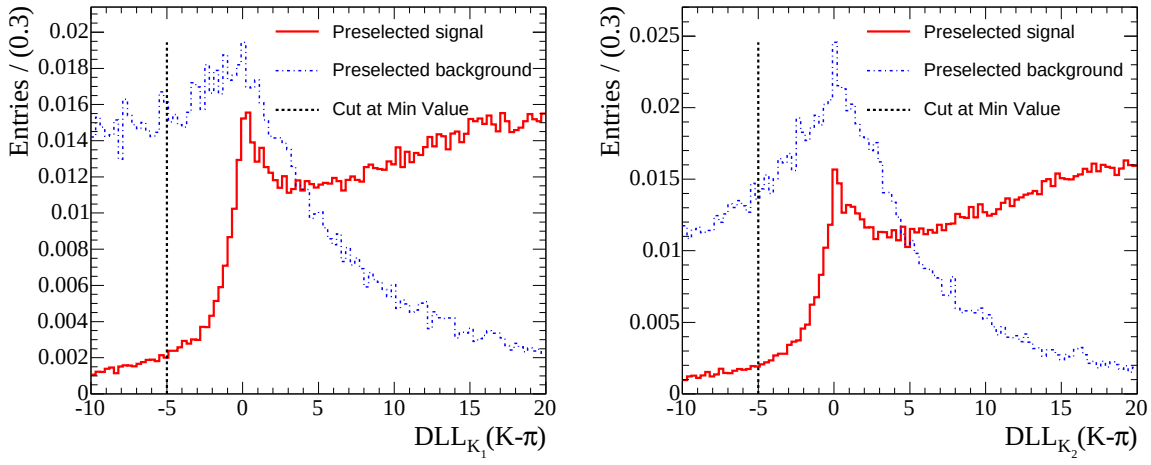

(a) $\mathrm{DLL}_{K^+}(K-\pi)$ (b) $\mathrm{DLL}_{K^-}(K-\pi)$.

FIG. 7: Cut on the identification of the kaons.

FS is then $\mathrm{FS}_{B_s-\mathrm{PV}} > 12$ (see Fig. 9 (c)). The fact that the B_s should point back to the primary vertex is further exploited here by requiring that $\cos(\theta_P) > 0.99997$ (defined in Eq. (24) and plotted in Fig. 9 (d)).

The most efficient cut is the cut on the reconstructed B_s mass. Cutting tight on this parameter would barely leave any event of background. But it is kept as loose as $|M_{B_s,\mathrm{reco}} - M_{B_s,\mathrm{true}}| < 500$ MeV/c^2 for the selection of the background (inclusive-$b\bar{b}$ data) to artificially increase the background statistics. The number of background events will then be counted in the loose mass window and downscaled to the tight mass window by dividing by the ratio of the two windows (10 in this case). On the other hand, the cut is tightened to $|M_{B_s,\mathrm{reco}} - M_{B_s,\mathrm{true}}| < 50$ MeV/c^2 for the signal. The distributions of this parameter and the two cuts are shown in Fig. 9 (e).

Table 4 summaries of all the cuts discussed in this Section (cuts for the final selection) and also shows the cuts that were used at the time of the TDR. Changes between the two analyses are shown in bold.

4.3 Results of the final selection

This section is dedicated to the presentation of the results of the final cuts presented above (Table 4) on the signal, inclusive-$b\bar{b}$, specific background and minimum-bias events. Section 4.3.3 presents how to downscale the level of background from the wide mass window to the tight mass window.

4.3.1 $B_s^0 \to D_s^- \pi^+$ events

The same sample of ∼4 M $B_s^0 \to D_s^- \pi^+$ events analysed for preselection has been analysed for this study in the tight mass window. For the purpose of calculating the efficiencies and the annual yield, a few subsets of the whole sample must be

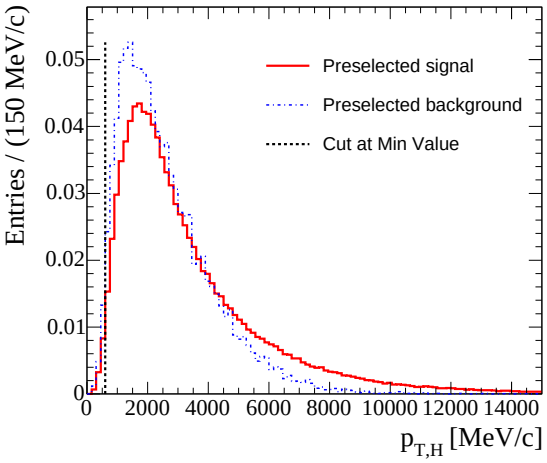

(a) p_T(bachelor)

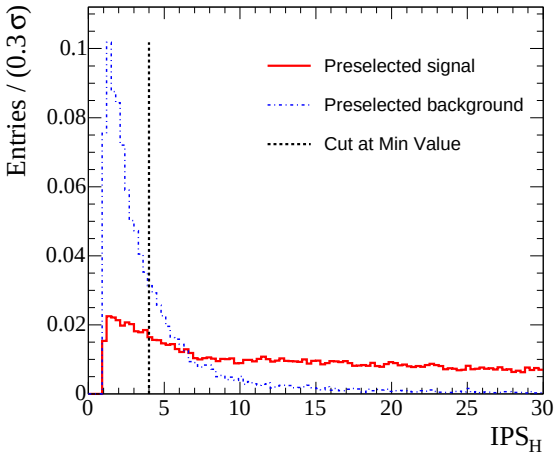

(b) IPS(bachelor)

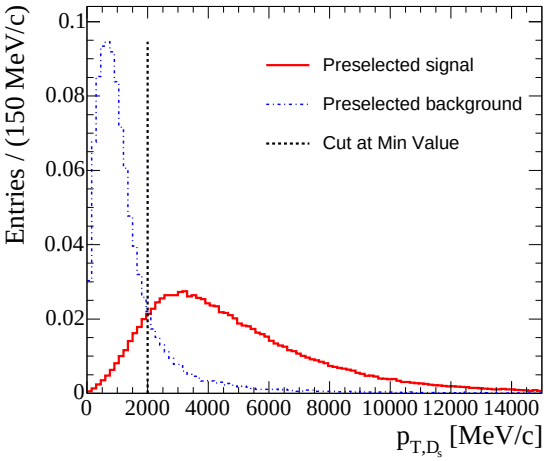

(c) $p_T(D_s)$

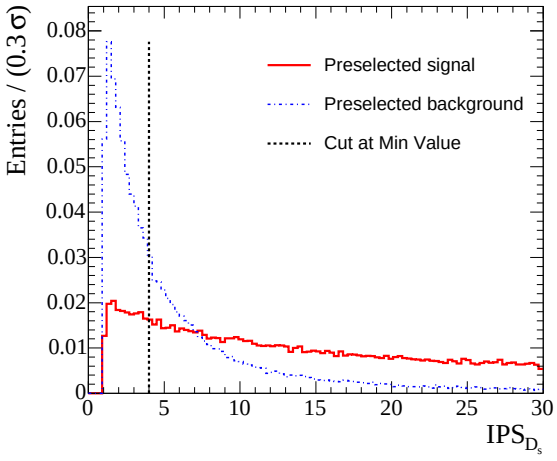

(d) IPS(D_s)

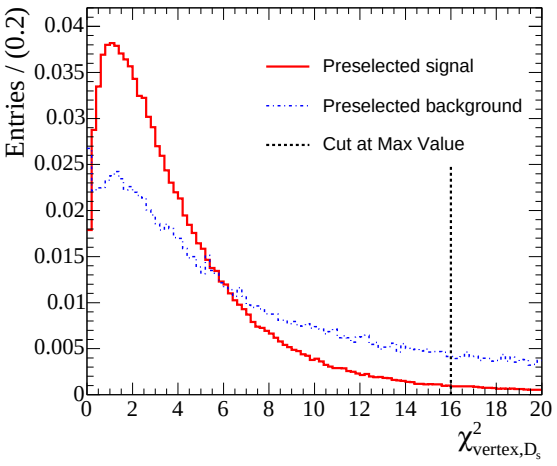

(e) $\chi^2_{D_s\ \mathrm{Vertex}}$

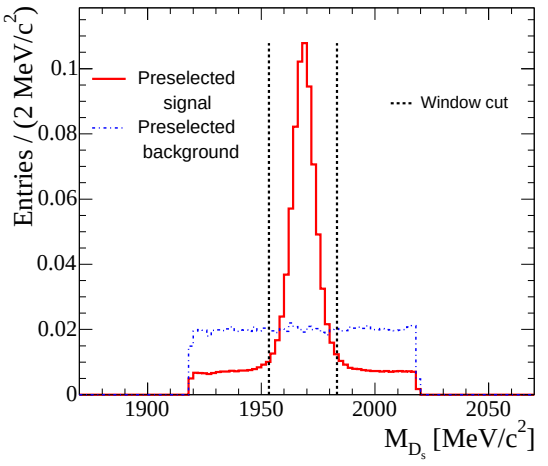

(f) M_{D_s}

FIG. 8: Cuts on the D_s and the bachelor parameters.

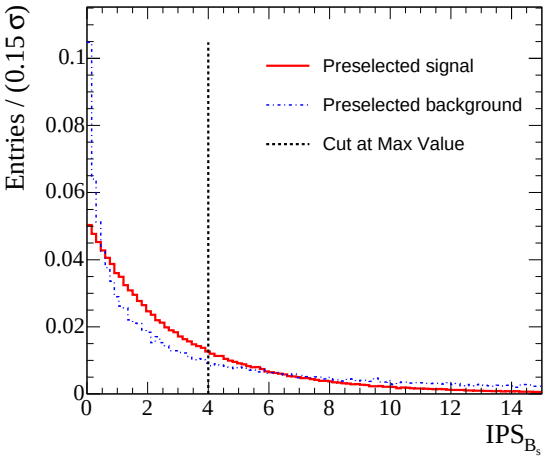

(a) IPS of the B_s

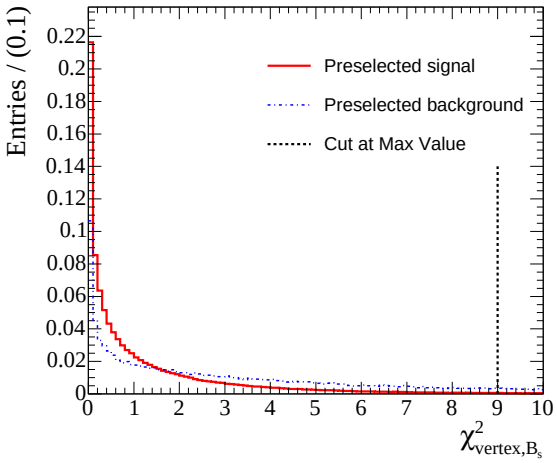

(b) $\chi_{B_s^2}$ Vertex

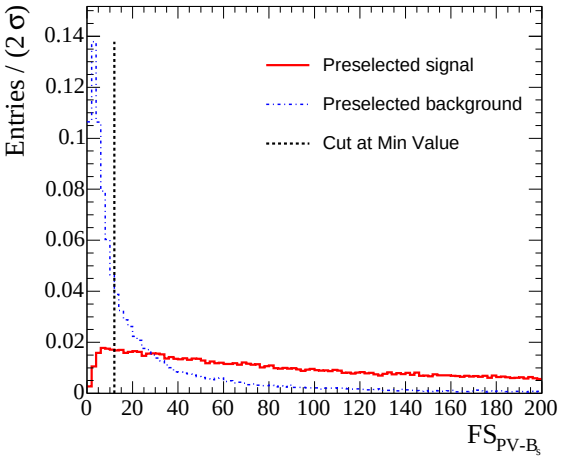

(c) FS between the PV and the B_s decay vertex

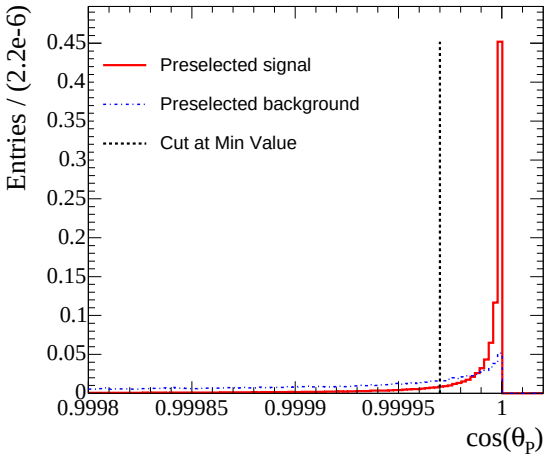

(d) $\cos(\theta_P)$

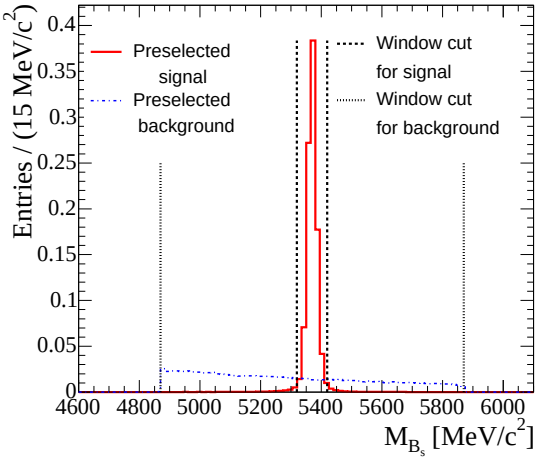

(e) Mass of the B_s

FIG. 9: Cuts on the B_s parameters.

TAB. 4: Final cuts on TDR and DC04 data. Changes between the two versions are written in bold font and changes between preselection and final cuts are written in italic font.

	TDR Final Cuts		DC04 Final Cuts	
Parameter	Min cut	Max cut	Min cut	Max cut
χ^2/NDF	—	4	—	—
P_H [GeV/c]	2	—	2	—
$P_{D_s\text{Prod}}$ [GeV/c]	2	—	2	—
p_{T,D_s} [MeV/c]	—	—	***2000***	—
$p_{T,H}$ [MeV/c]	700	—	***600***	—
$p_{T,D_s\text{Prod}}$ [MeV/c]	300	—	*300*	—
M_{B_s} [MeV/c^2] (l)	4869.6	5869.6	4869.6	5869.6
M_{B_s} [MeV/c^2] (t)	5319.6	5419.6	*5319.6*	*5419.6*
M_{D_s} [MeV/c^2]	1953.5	1983.5	*1953.5*	*1983.5*
IPS_{B_s}	—	3	—	***4***
IPS_{D_s}	2	—	***4***	—
IPS_H	4	—	*4*	—
$\text{IPS}_{D_s\text{Prod}}$	1	—	***3***	—
$\chi^2_{\text{Vertex}_{B_s}}$	—	3	—	***9***
$\chi^2_{\text{Vertex}_{D_s}}$	—	16	—	*16*
$\chi^2_{\text{Constr Vtx}_{D_s}}$	—	10	—	—
$\text{FS}_{D_s-\text{PV}}$	4.5	—	—	—
$\text{FS}_{B_s-\text{PV}}$	—	—	***12***	—
$z_{B_s} - z_{\text{PV}}$ [mm]	0	—	—	—
$z_{D_s} - z_{B_s}$ [mm]	0	—	0	—
$\cos(\theta_P)$	0.99997	—	*0.99997*	—
$\text{DLL}_H(\pi - K)$	-5	—	**-10**	—
$\text{DLL}_\pi(\pi - K)$	-5	—	**-10**	—
$\text{DLL}_K(K - \pi)$	-5	—	*-5*	—
$\text{DLL}_K(K - p)$	-5	—	**-10**	—
$\text{DLL}_K(K - e)$	-5	—	—	—

considered. Here are a few definitions of these subsets and how to count them:

N_{tot}**:** is the total number of events analysed for this study. This number is equal to the sum of the events stored on the analysed tapes.

N_{sel}**:** is the total number of events selected (not candidates), i.e. that passed all cuts.

$N_{\text{rec'ible}}$**:** is the number of reconstructible events as long tracks found in the whole sample. This number is not necessarily included in N_{sel}. This number is given by a dedicated algorithm (EffSelCheck v3r2, see Ref. [23]). A MC track is reconstructible as a long track if it can be measured both in the VeLo (at least

3 r and 3 ϕ hits) and in the T stations (at least 1 x and 1 stereo hit in each station T1-T3).

$N_{\text{rec'ed}}$**:** is the number of reconstructed events found in the whole sample. Note that $N_{\text{rec'ed}}$ is not a subset of $N_{\text{rec'ible}}$ as some events may be reconstructed but not reconstructible.

$N_{\text{rec'ible/ed}}$**:** is the number of events that are both reconstructible and reconstructed, again given by the EffSelCheck algorithm.

N_{trg}**:** is the number of selected events that have a positive trigger decision. The trigger decisions are saved in the n-tuples and include the number of events passing L0, passing L1 and passing L0 and L1. The sample of events that pass L1 is not a subset of the sample that passes L0 (i.e. some events may pass L1 but not L0). The version used for the trigger is L0DU v6r7p2 and TrgSys v1r1.

N_{tag}**:** is the number of tagged events. This number is given by the Flavour Tagging algorithm (v5r3). This algorithm gives as output the number of events tagged (separated into the different tpyes of tag, e.g. same side π tag or opposite side tag) and the three important values for this study: the tagging efficiency (ϵ_{tag}), the wrong tag fraction (ω) and the effective combined tagging efficiency (ϵ_{eff}).

Table 5 shows the summary of all these numbers. They will be used in Sections 5.1 and 5.2. The number of independent events is calculated using Eq. (19-21). The fraction of independent events in the sample is

$$f_{\text{indep}}^{\text{signal}} = (89.01 \pm 0.09)\%.$$

TAB. 5: Numbers of events of signal in the tight mass window: analysed, selected, reconstructible, reconstructed, reconstructible and reconstructed, and triggered events, tagging efficiency and wrong tag fraction after L0 and L1.

	Total	Independent
N_{tot}	$3.9855 \cdot 10^6$	$3.54747 \cdot 10^6$
N_{sel}	142726	127040
$N_{\text{rec'ible}}$	591281	526296
$N_{\text{rec'ed}}$	565506	503354
$N_{\text{rec'ible/ed}}$	465577	414408
N_{trg}	52662	46874
ϵ_{tag}	$(56.17 \pm 0.18)\%$	
ω	$(33.53 \pm 0.15)\%$	
ϵ_{eff}	$(6.10 \pm 0.19)\%$	

4.3.2 Minimum-bias events

The same selection (with the set of final cuts defined in Table 4) has been applied to a sample of minimum-bias events. The whole initial sample included 12773303 events (which represents one second of data taking when the experiment will be running). This sample has been submitted to both the L0 and L1 trigger algorithms. Out of this sample, 785658 events were L0-accepted and 31752 were L0 and L1-accepted. The selection was then applied to this 31752 L0 and L1 accepted events. No events were selected. If one event had been selected (i.e. one event of background per second), the signal would have been invisible in the background.

4.3.3 Inclusive-$b\bar{b}$ events

A total sample of 20.5 M inclusive-$b\bar{b}$ events has been analysed for this study of the background. The fraction of independent events in this sample, calculated using Eq. (19-21) is

$$f_{\text{indep}}^{b\bar{b}} = (57.98 \pm 0.02)\%.$$

Out of these 20.3M events ($\sim$11.8 $\cdot 10^6$ independent) 106 independent were selected in the loose mass window. These selected events must then be analysed one by one to check whether they must be counted as background or not. For this purpose, the decay trees are printed for both the reconstructed B_s and the true b hadrons found in the event (B_s^0, $\bar{B}_s^0$, B^0, $\bar{B}^0$, $B^\pm$, Λ_b^0, $\bar{\Lambda}_b^0$ and $B_c^\pm$). Below is a list of the different type of events that can be selected:

True signal: the $B_s^0 \to D_s^- \pi^+$ events should not be counted as background events.

Incompletely reconstructed specific background events: some specific background decays are reconstructed in the wide mass window. However, some of these will never be reconstructed in the tight mass window because one particle is missing in the reconstruction of the decay (e.g. the γ or the π^0 in $B_s^0 \to D_s^* \pi$ or the ν in $B_s^0 \to D_s l \nu$ can have a hard enough mass spectrum). These should therefore not be counted as background.

Completely reconstructed specific background events: some other specific decays are fully reconstructed in the tight mass window ($B_d^0 \to D^\pm \pi^\mp$ and $\Lambda_b \to \Lambda_c \pi$) with a mis-identified pion. These events must be counted as real background events.

Combinatorial background: some events are reconstructed using tracks that come from different decays. Whether there is a true D_s reconstructed and the bachelor doesn't come from the same B-meson, or if all tracks come from unknown decays, these combinations are counted as real background.

Tables 6 and 7 are summaries of the events of all different types found in the 106 independent events selected in the wide mass window. The total number of 45 real background events is used in the calculation of the background-to-signal ratio (see Section 5.1.4.

TAB. 6: List of the different types of background events selected and total number of real independent background events.

Event type	Independent	Total
True Signal	10	11
Incomplete reconstruction	51	75
Real b events + misidentification	**6**	**6**
Combinations	**39**	**42**
Real BKG	**45**	**48**

TAB. 7: Detailed list of all the inclusive-$b\bar{b}$ independent selected events.

Decay found	Independent	Total
True signal		
$B_s \to D_s\pi$	10	11
Incomplete reconstruction		
$B \to Da_1$	1	1
$B \to D$(semi-leptonic)π	1	1
$B \to D\rho$	5	5
$B \to D^* l\nu$	2	5
$B \to D^*\pi$	2	4
$B \to D^*\pi\pi$	1	2
$B \to D^*\rho$	3	4
$B \to D_s\pi$	1	2
$B \to D_s\rho$	1	3
$B_s \to D_s a_1$	1	3
$B_s \to D_s l\nu$	2	3
$B_s \to D_s\pi\pi$	1	2
$B_s \to D_s\rho$	4	6
$B_s \to D_s^* l\nu$	4	4
$B_s \to D_s^*\pi$	12	16
$B_s \to D_s^*\pi\pi$	2	2
$B_s \to D_s^*\rho$	2	4
$\Lambda_b \to D_s p$	2	4
$\Lambda_b \to D_s^* p$	2	2
$\Lambda_b \to \Lambda_c\rho$	1	1
$\Lambda_b \to \Sigma_c\pi$	1	1
Real b events + misidentification		
$B \to D\pi$	4	4
$\Lambda_b \to \Lambda_c\pi$	2	2

Figure 10 (a) and (b) show the distribution of the reconstructed B_s mass and proper time, respectively, for the 106 independent inclusive-$b\bar{b}$ events selected in the loose mass window. The left plot shows the peak inside the tight mass window which is due to the true signal events and the "Real b events + misidentification" ones. Also on the lower side of the distribution, a peak is visible which corresponds to the "incomplete reconstruction" events.

The right plot shows that the background events have a proper time that peaks at low τ.

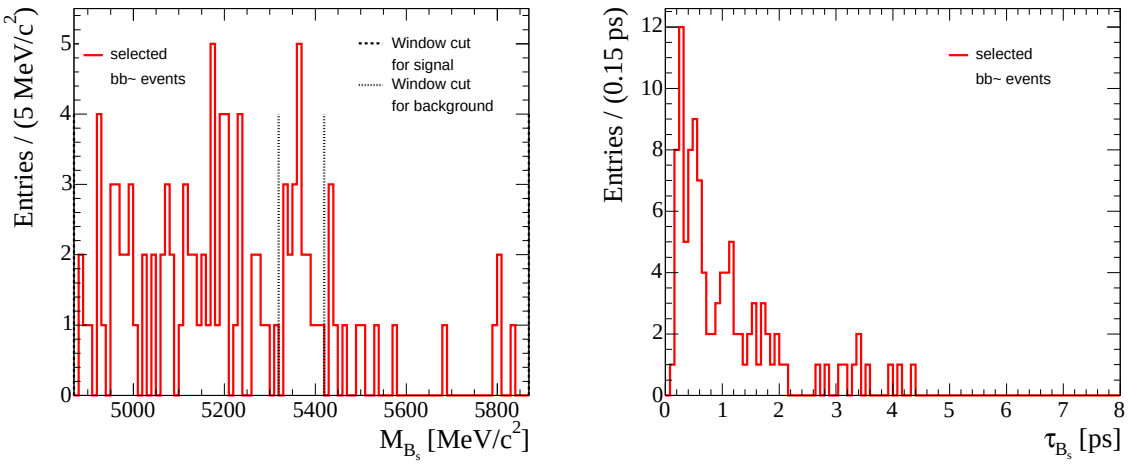

(a) Reconstructed B_s mass, (b) Reconstructed B_s proper time.

FIG. 10: Reconstructed B_s mass and proper time (τ) of the selected inclusive-$b\bar{b}$ events.

4.3.4 Specific backgrounds events

A further analysis of 110k $B_d^0 \to D^-\pi^+$ events has been performed after a first look at the events of $b\bar{b}$ passing the selection. The misidentification of a π coming from the D-meson leads to a reconstructed mass inside the tight mass window.

The tight selection has been applied to this specific background decay. The results show that 151 events are selected out of the 110k events initial sample. This result will be used in Section 5.1.5 to calculate the contribution of this specific decay to the background-to-signal ratio.

Figure 11 shows the reconstructed B_s mass of the selected $B_d^0 \to D\_\pi^+$ events (loose mass window). It is visible on this plot that the distribution of the mass does not peak completely inside the tight mass window. Thus only the events inside the tight mass window have been counted to calculate the B/S in Section 5.1.5.

The mean of the destribution shown in Fig. 11 is $< M_{B_s,\text{reco}} >= 5335$ MeV/c^2 which falls between the true mass of the B_s meson (~ 5370 MeV/c^2) and the true mass of the B_d (~ 5279MeV/c^2) meson due to the misidentification of a pion coming from the D meson as a kaon.

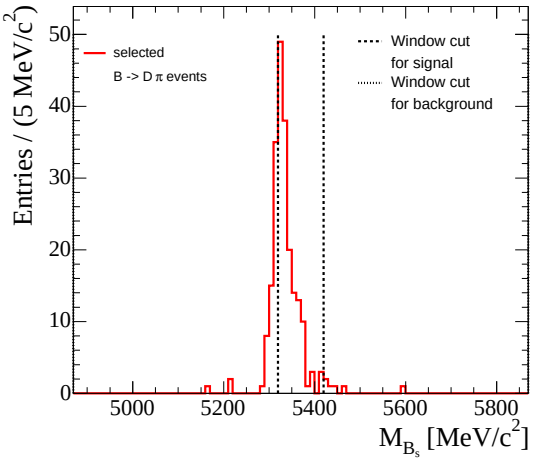

FIG. 11: Reconstructed B_s mass of the selected $B_d \to D^-\pi^+$ events.

4.4 New set of cuts for a better preselection

For the purpose of a faster analysis, a preselection is applied on the background data tapes. This so-called stripping rejects a large number of events. The convention is that, if the calculated rejection factor is smaller than 1000, then a downscaling is applied to the remaining sample that removes events arbitrary until the 1000 factor is reached. This needs to be avoided.

Using the set of preselection cuts defined in Section 4.1 on a first sample of 1881398 independent events analysed, there are 28976 events that pass the preselection. This gives a rejection factor of

$$\mathcal{R} = \frac{1881398}{27319} \simeq 69 \pm 1$$

which is clearly not enough.

The error is here calculated as

$$\sigma_{\mathcal{R}} = \sqrt{\frac{(N-n)N}{n^3}}$$

where N is the number of independent events analysed and n is the number of independent preselected events.

The strategy to get a rejection factor of 1000 is to slightly tighten some of the preselection cuts (defined in Section 4.1) until this result is obtained. These cuts also have to be looser than the final cuts shown in Section 4.3. The loosest cuts were tightened and the rejection factor was calculated. This operation was then repeated until the wanted result was reached.

Table 8 summarizes the three set of cuts discussed so far, which are the set of cuts used for the preselection for this study, the set of cuts for the final selection of all events and the set of cuts proposed for a stripping with an intrinsic rejection factor of more than 1000 (no need for any arbitrary downscaling).

TAB. 8: Summary of used preselection cuts, proposed preselection cuts and final cuts. Changes between two columns are written in bold font.

	Used Preselection		New Preselection		Final Cuts	
Parameter	Min cut	Max cut	Min cut	Max cut	Min cut	Max cut
P_H [GeV/c]	2	—	2	—	2	—
$P_{D_s\text{Prod}}$ [GeV/c]	2	—	2	—	2	—
p_{T,D_s} [MeV/c]	0	—	**500**	—	**2000**	—
$p_{T,H}$ [MeV/c]	200	—	**300**	—	**600**	—
$p_{T,D_s\text{Prod}}$ [MeV/c]	200	—	**300**	—	300	—
M_{B_s} [MeV/c^2] (l)	4869.6	5869.6	4869.6	5869.6	4869.6	5869.6
M_{B_s} [MeV/c^2] (t)	4869.6	5869.6	4869.6	5869.6	**5319.6**	**5419.6**
M_{D_s} [MeV/c^2]	1918.5	2018.5	**1938.5**	**1988.5**	**1953.5**	**1983.5**
IPS_{B_s}	—	20	—	**16**	—	**4**
IPS_{D_s}	1	—	**2**	—	**4**	—
IPS_H	1	—	1	—	**4**	—
$\text{IPS}_{D_s\text{Prod}}$	0	—	**1**	—	**3**	—
$\chi^2_{\text{Vertex}_{B_s}}$	—	10	—	10	—	**9**
$\chi^2_{\text{Vertex}_{D_s}}$	—	20	—	20	—	**16**
$\text{FS}_{B_s-\text{PV}}$	0	—	0	—	**12**	—
$z_{D_s} - z_{B_s}$ [mm]	0	—	0	—	0	—
$\cos(\theta_P)$	0.9995	—	0.9995	—	**0.99997**	—
$\text{DLL}_H(\pi - K)$	-10	—	-10	—	-10	—
$\text{DLL}_\pi(\pi - K)$	-10	—	-10	—	-10	—
$\text{DLL}_K(K - \pi)$	-10	—	**-5**	—	-5	—
$\text{DLL}_K(K - p)$	-10	—	-10	—	-10	—

Using these cuts, the rejection factor becomes

$$\mathcal{R} = \frac{1881398}{1853} \simeq 1016 \pm 24$$

which is consistent with 1000.

5 Results

In this section are presented all the results of the complete analysis. The first subsection presents all the efficiencies of selection and rejection, the annual signal yield and the background-to-signal ratio (due to inclusive-$b\bar{b}$ events) calculated with the data selected using the tuned set of cuts. The next subsections present the results for the calculation of two physics parameters: the wrong tag fraction ω and the resolution on the difference in mass of the two mass eigenstates: $\sigma_{\Delta m_s}$. Then some further analyses on the data will be presented: an analysis on the proper time

resolution, a study of the proper time pull and a presentation of the acceptance before and after trigger.

The errors on the efficiencies have been calculated with the assumption that the denominator is a subset of the numerator (dependent numbers). Also, as discussed in Section 3.2.1, the numbers of independent events are used for this calculation. If the efficiency is calculated as

$$\epsilon = \frac{N_1}{N_2},$$

then the error on the efficiency is calculated as:

$$\sigma_\epsilon = \frac{\sqrt{\epsilon(1-\epsilon)}}{N_2}$$

5.1 Efficiencies, yield and background for the $B_s^0 \to D_s^- \pi^+$ decay

In this section, the results found for the final selection in Section 4.3 are used to calculate the selection efficiency of signal and background, the trigger efficiency, the annual signal yield and the B/S ratio.

5.1.1 Efficiencies

Different efficiencies must be calculated to get the total efficiency. The detector efficiency (ϵ_{det}, which will be calculated at the end) is made of the angular acceptance of the detector and the fraction of events that are reconstructible. The reconstruction efficiency is

$$\epsilon_{\text{rec/det}} = \frac{N_{\text{rec'ible/ed}}}{N_{\text{rec'ible}}} \tag{25}$$

where the different numbers used have been defined in Section 4.3.1. Then the selection efficiency can be defined as

$$\epsilon_{\text{sel/rec}} = \frac{N_{\text{sel}}}{N_{\text{rec'ed}}}. \tag{26}$$

These two equations, along with ϵ_{det} can be combined to calculate the total offline selection efficiency

$$\epsilon_{\text{off}} = \epsilon_{\text{det}} \times \epsilon_{\text{rec/det}} \times \epsilon_{\text{sel/rec}} = \frac{N_{\text{sel}}}{N_{\text{tot}}} \times \epsilon_\theta \tag{27}$$

where ϵ_θ is the fraction of events where the signal b-hadron is in the angular acceptance (400 mrad). Its value for the TDR was

$$\epsilon_\theta = (34.71 \pm 0.03)\% \tag{28}$$

This value is assumed to be the same for the new data. From these definitions, the detection efficiency can be calculated as

$$\epsilon_{\text{det}} = \frac{\epsilon_{\text{off}}}{\epsilon_{\text{rec/det}} \times \epsilon_{\text{sel/rec}}} \tag{29}$$

Finally, the trigger efficiency is calculated

$$\epsilon_{\mathrm{trg/sel}} = \frac{N_{\mathrm{trg}}}{N_{\mathrm{sel}}} \tag{30}$$

and all these efficiencies are combined together to get the total efficiency

$$\epsilon_{\mathrm{tot}} = \epsilon_{\mathrm{det}} \times \epsilon_{\mathrm{rec/det}} \times \epsilon_{\mathrm{sel/rec}} \times \epsilon_{\mathrm{trg/sel}} = \epsilon_{\mathrm{off}} \times \epsilon_{\mathrm{trg/sel}}. \tag{31}$$

The values of all these efficiencies, using the numbers of Table 5, are shown in Table 9.

TAB. 9: Summary of the signal efficiencies for the DC04 $B_s^0 \to D_s^- \pi^+$ data. For comparison, also the efficiencies as presented in the TDR are given.

Data	Factors (in %) forming ϵ_{tot} (in %) $\epsilon_{\mathrm{tot}} = \epsilon_{\mathrm{det}} \times \epsilon_{\mathrm{rec/det}} \times \epsilon_{\mathrm{sel/sec}} \times \epsilon_{\mathrm{trg/sel}}$				
	ϵ_{det}	$\epsilon_{\mathrm{rec/det}}$	$\epsilon_{\mathrm{sel/rec}}$	$\epsilon_{\mathrm{trg/sel}}$	ϵ_{tot}
TDR	5.36 ± 0.05	80.6 ± 0.3	25.0 ± 0.4	31.1 ± 0.8	0.337 ± 0.008
DC04	6.255 ± 0.011	78.74 ± 0.06	25.24 ± 0.08	36.90 ± 0.14	0.4586 ± 0.0021

To compare the results found on the new data with those found for the TDR, two more efficiencies can be defined: the selection efficiency (including the reconstruction) and the rejection efficiency

$$\epsilon_{\mathrm{sel}} = \frac{N_{\mathrm{sel}}(\mathrm{signal})}{N_{\mathrm{tot}}(\mathrm{signal})} \qquad \epsilon_{\mathrm{rej}} = 1 - \frac{N_{\mathrm{sel}}(b\bar{b})}{N_{\mathrm{tot}}(b\bar{b})}$$

At the time of the TDR data, a sample of 196.5 k signal events and 5.2 M inclusive-$b\bar{b}$ events had been analysed [5]. Applying the selection criteria resulted in a total of $N_{\mathrm{sel}}(\mathrm{signal}) = 6125$ selected signal events in the tight mass window and $N_{\mathrm{sel}}(b\bar{b}) = 32$ selected background events in the wide mass window (with only 10 events of real background). These results lead to

$$\epsilon_{\mathrm{sel}} = (3.117 \pm 0.039)\%$$
$$\epsilon_{\mathrm{rej}} = 99.99938\% \pm 1.1 \cdot 10^{-6}$$

With the results from the new data, the efficiencies are

$$\epsilon_{\mathrm{sel}} = (3.581 \pm 0.010)\%$$
$$\epsilon_{\mathrm{rej}} = 99.99934\% \pm 7.5 \cdot 10^{-7}$$

The efficiency of selection with the new generation of data and the new set of cuts has increased by ∼13% (relative). This is important as it increases the annual signal yield (see Section 5.1.3). But the other important value to check is the background-to-signal ratio (B/S). This value will be calculated in chapter 5.1.4.

5.1.2 $D_s^-\pi^+$ vs $D_s^+\pi^-$

A study has been performed on the selected events to check whether there is a difference in the efficiency of selection between $D_s^-\pi^+$ and $D_s^+\pi^-$. The simple test consists in checking whether the bachelor is a π^+ ($B_s^0 \to D_s^-\pi^+$) or a π^- ($\bar{B}_s^0 \to D_s^+\pi^-$). So each of the numbers defined above are separated into two subsets (which are summed to get the results in Table 5). It is assumed here (knowing the parameters from the generation) that the events generated are 50% $B_s^0 \to D_s^-\pi^+$ and the other half is $\bar{B}_s^0 \to D_s^+\pi^-$. Using this assumption, the efficiencies of selection ($\frac{N_{\rm sel}}{N_{\rm tot}}$) are calculated for each subset. The calculation shows that the selection is slightly more efficient for the $D_s^-\pi^+$ than for the $D_s^+\pi^-$:

$$\epsilon_{\rm sel}^{D_s^-\pi^+} = (3.60 \pm 0.01)\%$$

$$\epsilon_{\rm sel}^{D_s^+\pi^-} = (3.56 \pm 0.01)\%$$

The difference between these two efficiencies is $\Delta\epsilon = (0.040 \pm 0.014)\%$ which corresponds to a 3σ error. This difference is therefore not really significant.

5.1.3 Annual signal yield

The annual signal yield ($N_{\rm phys}$) is the number of selected, reconstructed and triggered events in one year of data taking (without tagging nor HLT). This number is calculated by multiplying the number of events produced in one year by the total efficiency

$$N_{\rm phys} = \mathcal{L}_{\rm int} \times \sigma_{b\bar{b}} \times (2 \times f_{B_s}) \times {\rm BR}_{\rm vis} \times \epsilon_{\rm tot}, \tag{32}$$

where $\mathcal{L}_{int}$ is the annual integrated luminosity ($2\times10^{32}{\rm cm}^2{\rm s}^{-1}$ for 10^7 s per year), $\sigma_{b\bar{b}}$ is the assumed $b\bar{b}$ production cross-section of $500\mu b$, f_{B_s} is the fraction of $\bar{b}$-quarks which produce a B_s^0-meson ($(10.0 \pm 1.3)\%$) and the factor 2 takes into account that in a $b\bar{b}$ event, there are two b-quarks that can produce a B_s-meson. Finally ${\rm BR}_{\rm vis}$ is the visible branching ratio of the full decay $B_s^0 \to (D_s^- \to K^+K^-\pi^-)\pi^+$ which has been given in Table 1.

The error on the annual signal yield is calcuated taking into account only the statistical errors. So the systematic uncertainty on the visible branching ratio is not taken into account.

The result for the annual yield, with the efficiencies found in this study, is (111.4 $\pm$ 0.5) k events reconstructed, selected and triggered (compared to 81.7 k for the TDR data). This amount will need to be downscaled by the efficiency of HLT. As discussed before, it is not known yet but an estimate of what will be achieved is around 85%. The result that is interesting for this study is that the annual signal yield has been increased by $\sim$36% (relative) since the time of the TDR.

5.1.4 B/S from combinatorial background

Finally, the other interesting value to calculate is the background-to-signal ratio, which indicates the background level under the signal mass peak. It is assumed

that the "real" inclusive-$b\bar{b}$ background events are evenly distributed in the loose B_s mass window to artificially increase the statistics (this assumption can be checked in Fig. 9 (e)). This B/S ratio is defined as

$$\frac{B}{S} = \frac{N_{\rm phys}(b\bar{b})}{N_{\rm phys}({\rm signal})} = \frac{\mathcal{L}_{int} \times \sigma_{b\bar{b}} \times \epsilon_{\theta/b\bar{b}} \times \epsilon_{{\rm sel}/b\bar{b}} \times \frac{1}{10}}{\frac{N_{\rm phys}({\rm signal})}{\epsilon_{\rm trg/sel}}} \tag{33}$$

where $\epsilon_{\theta/b\bar{b}}$ is the fraction of generated $b\bar{b}$ events where one of the b-hadrons is in the geometrical acceptance of the detector ($\epsilon_{\theta/b\bar{b}} = (43.21 \pm 0.04)\%$ at the time of the TDR), $\epsilon_{sel/b\bar{b}}$ is the efficiency of selection of the $b\bar{b}$ events (with $N_{sel}(b\bar{b}) = 39$, the number of independent combinatorial background events), the result is given before trigger [8] and the $\frac{1}{10}$ factor comes from the downscale of the mass window from the loose cut (± 500 MeV/c^2) to the tight cut (± 50 MeV/c^2) [9].

Using the results given above, the estimated B/S ratio due to the combinatorial background only is

$$\left(\frac{B}{S}\right)^{\rm combinatorial}_{B_s \to D_s \pi} = 0.47 \pm 0.08 \tag{34}$$

The error is again calculated with the propagation of the statistical (gaussian) errors only (no systematic uncertainty included).

5.1.5 B/S from specific background

The contribution to B/S due to the specific backrgound must also be calculated. These events can not be considered to be evenly distributed in the loose mass window and the contribution must hence be calculated by studying only the events that pass the tight mass selection. The study on the $B^0_d \to D^-\pi^+$ decay has shown that 151 events are selected out of an initial sample of 110k events. Using the visible branching ratio for this decay ($\mathrm{BR}^{B^0_d \to D^-\pi^+}_{\rm vis} = 254 \cdot 10^{-6}$) and the fraction of b quarks forming a B_d meson, the B/S due to $B^0_d \to D^-\pi^+$ can be calculated:

$$\left(\frac{B}{S}\right)^{B_d \to D\pi}_{B_s \to D_s \pi} = \left(\frac{f_{B_d}}{f_{B_s}}\right) \left(\frac{\mathrm{BR}_{{\rm vis},B_d \to D\pi}}{\mathrm{BR}_{{\rm vis},B_s \to D_s\pi}}\right) \left(\frac{\epsilon_{{\rm tot},B_d \to D\pi}}{\epsilon_{{\rm tot},B_s \to D_s\pi}}\right)$$

where $f_{B_d} = 0.39$ and $f_{B_s} = 0.10$ are the fractions of b quarks hadronising to a B_d and B_s meson respectively, BR_{vis} is the visible branching ratio (i.e. the branching ratio of the overall $B^0_d \to (D^- \to K^-\pi^+\pi^+)\pi^+$ and $B^0_s \to (D^-_s \to K^+K^-\pi^-)\pi^+$) and $\epsilon_{\rm tot}$ is the total efficiency (detection, reconstruction and selection). The B/S is calculated before trigger.

This analysis has shown that this specific background can induce a background-to-signal ratio as high as

$$\left(\frac{B}{S}\right)^{B_d \to D\pi}_{B_s \to D_s \pi} = 0.31 \pm 0.03.$$

[8] Note that if the trigger efficiency is the same for both the signal and the background data, then B/S is the same before and after trigger.

[9] If the number of real background events had been smaller than 10, B/S would have ben given as an interval using a 90% confidence level.

This ratio could probably be reduced by cutting tighter on the PID of the tracks. Unfortunately this new consideration cannot be tested as part of this master thesis.

The second specific background found in the inclusive-$b\bar{b}$ sample that has a contribution to the B/S is the $\Lambda_b^0 \to (\Lambda_c^+ \to pK^-\pi^+)\pi^-$ decay. As discussed previously, this decay couldn't be studied as no data has been generated. The B/S contribution can still be estimated. If the assumption is made that the Feynman's diagrams for $B_d \to D\pi$ and for $\Lambda_b \to \Lambda_c\pi$ are approximately the same, then the contribution to B/S due to this specific background can be approximated as

$$\left(\frac{B}{S}\right)^{\Lambda_b\to\Lambda_c\pi}_{B_s\to D_s\pi} = \left(\frac{f_{\Lambda_b}}{f_{B_d}}\right)\left(\frac{\mathrm{BR}_{\Lambda_c^+\to pK^-\pi^+}}{\mathrm{BR}_{D^-\to K^-\pi^+\pi^+}}\right)\left(\frac{B}{S}\right)^{B_d\to D\pi}_{B_s\to D_s\pi}$$

where $f_{\Lambda_b} = 0.12$ is the fraction of b quarks hadronising to Λ_b baryon and $\mathrm{BR}_{\Lambda_{c^+}\to pK^-\pi^+} = 5\%$.

Using the numbers above, this contribution to the background-to-signal ratio becomes:

$$\left(\frac{B}{S}\right)^{\Lambda_b^0\to\Lambda_c^+\pi^-}_{B_s^0\to D_s^-\pi^+} = 0.05 \pm 0.01.$$

5.1.6 Total B/S

The total background-to-signal ratio can then be calculated as the sum of three contributions discussed above. This leads to

$$\left(\frac{B}{S}\right)^{\mathrm{tot}}_{B_s\to D_s\pi} = 0.83 \pm 0.09.$$

Tables 9 and 10 show the summary for the efficiencies, the annual signal yield and the B/S calculated above.

Another method has also been used to calculate this B/S to get a result comparable to the result shown in the TDR. This second method doesn't take into account that the events are not independent. Also, the specific background events (called "real b events and misidentification" above) are supposed to be evenly distributed in the loose mass window. The number of events studied is then 48 (= 45 + 3 doubles). In this case, the background-to-signal ratio becomes

$$\left(\frac{B}{S}\right) = 0.34 \pm 0.05.$$

5.2 Physics performances

As described in the introduction (Section 2.5) about the $B_s^0 \to D_s^-\pi^+$ decay, there are three parameters that can be calculated using this channel: ω, ΔM_s and $\Delta\Gamma_s$. In this section, the wrong tag fraction ω (and also the tagging efficiency and effective tagging efficiency) will be calculated as well as the sensitivity to ΔM_s: $\sigma_{\Delta M_s}$.

TAB. 10: Summary of the untagged annual signal yields (after trigger) and background-over-signal (B/S) ratios (before trigger) for $B_s^0 \to D_s^- \pi^+$ at the time of the TDR and with the new DC04 data. The annual signal yields include both the indicated decay and its charge conjugate. Quoted errors on B/S are from the Monte Carlo statistics.

Data	Assumed BR_{vis} (in 10^{-6})	Annual signal yield	B/S ratio from incl. $b\bar{b}$ back.
TDR	120 ± 30	(81.7 ± 1.9)k	0.32 ± 0.10
DC04	120 ± 30	(111.4 ± 0.5)k	0.83 ± 0.09

5.2.1 Tagging performances

Using the code released with the tagging algorithm the tagging efficiency, the wrong tag fraction, and the combined effective tagging efficiency can be calculated before the triggers, after L0 and after L0 and L1. These results are shown in Table 11. The detailed results of the tagging analysis can be found in Appendix B.

TAB. 11: Tagging efficiency, wrong tag fraction and effective combined tagging efficiency before triggers, after L0 and after L0&L1

	Before Triggers	After L0	After L0&L1
ϵ_{tag}	(51.17±0.09)%	(54.64±0.14)%	(56.17±0.18)%
ω	(36.34±0.09)%	(34.34±0.13)%	(33.53±0.15)%
ϵ_{eff}	(3.82±0.08)%	(5.36±0.15)%	(6.10±0.19)%

The efficiencies calculated after the trigger are:

$$\epsilon_{\text{tag}} = (56.17 \pm 0.18)\%, \qquad \omega = (33.53 \pm 0.15)\%,$$

and

$$\epsilon_{\text{eff}} = (6.10 \pm 0.19)\%$$

Compared to the studies done for the TDR, both the tagging efficiency and the wrong tag fraction have increased. In the former studies, the results were

$$\epsilon_{\text{tag}} = (54.6 \pm 1.2)\%, \qquad \omega = (30.0 \pm 1.6)\%,$$

and

$$\epsilon_{\text{eff}} = (8.7 \pm 1.2)\%$$

after trigger which are close the results obtained in this study.

5.2.2 Sensitivity to ΔM_s

One of the motivations for studying the $B_s^0 \to D_s^- \pi^+$ is to measure ΔM_s, which is responsible for the B_s^0-meson oscillation. The statistical significance on this parameter is given by (Ref. [22])

$$\mathcal{S} \approx \sqrt{\frac{N_{\rm tag}}{2}} \cdot f_{\rm sig} \cdot (1 - 2\omega_{\rm tag}) \cdot e^{\frac{-(\Delta M_s \sigma_\tau)^2}{2}} = \sqrt{\frac{N_{\rm phys}}{2} \cdot \epsilon_{eff}} \cdot f_{\rm sig} \cdot e^{\frac{-(\Delta M_s \sigma_\tau)^2}{2}} \qquad (35)$$

where $\mathcal{S}$ is the average statistical significance on the amplitude of the B_s^0-$\bar{B}_s^0$ oscillations, $N_{\rm tag}$ is the number of tagged events, $N_{\rm phys}$ is the annual signal yield, $f_{\rm sig}$ is the fraction of signal in the sample

$$f_{\rm sig} = \frac{1}{1 + \frac{B}{S}}$$

ω_{tag} is the wrong tag fraction, $\epsilon_{\rm eff}$ is the combined effective tagging efficiency, ΔM_s is the difference in mass between the two mass eigenstates and σ_τ is the resolution on the proper time.

It appears that this significance decreases quickly with increasing values of ΔM_s and is very sensitive to the proper time resolution σ_t which makes it a very important parameter (a good proper time resolution is required to resolve the fast B_s^0-$\bar{B}_s^0$ oscillations).

Figure 12 shows this significance for a 10% interval around the central value of the proper time resolution calculated using a double gaussian ($\sigma_{\tau_{B_s}} = 42.0$ fs, see Section 5.3.4).

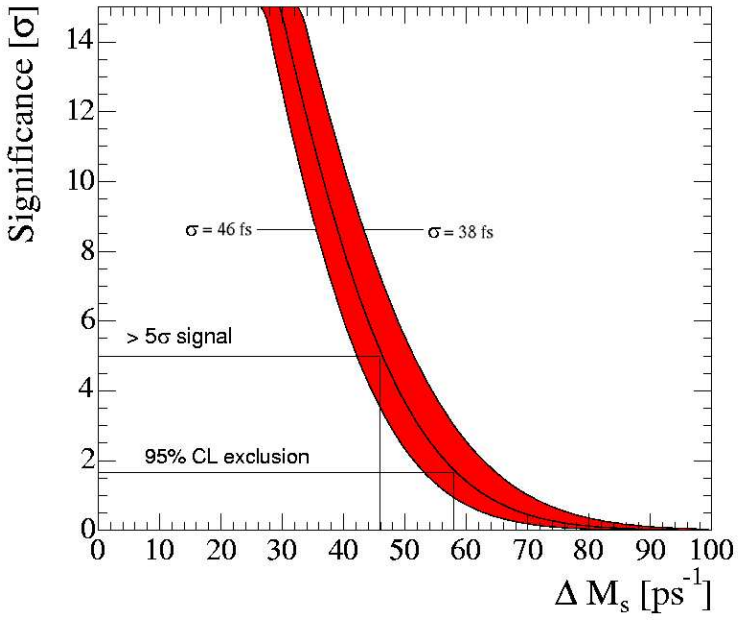

FIG. 12: The one year sensitivity to ΔM_s for a proper time resolution of 42.0 fs $\pm$ 10%.

This plot shows that a 5σ measurement of ΔM_s will be possible for values up to 46 ps^{-1} after one year of data taking. Also it shows that all values smaller than 58 ps^{-1} can be excluded with a confidence level of 95%. Using the TDR numbers to this equation (see Section C) shows that an improvement of 1 ps^{-1} has been obtained for the 5σ measurement. In fact, this sensitivity to ΔM_s should be calculated using a toy Monte Carlo simulation that takes into account the event-by-event error. This was done for the TDR and the analysis had shown that a 5σ measurement was possible up to 68ps^{-1}. This analysis cannot be performed as part of this master thesis but this last result shows that a more complete analysis would give better results.

Different tagging algorithms are combined using neural nets. These algorithms are much more efficient than the common ones used for this study. It appeared that the combined effective tagging efficiency for the $B_s^0 \to D_s^- \pi^+$ decay could increase to $\epsilon_{\text{eff}} = 9.2\%$ instead of $\epsilon_{\text{eff}} = 6.10\%$ used in this analysis (see Ref. [24]). In this case, the 5σ measurement of ΔM_s would be possible for values up to 48 ps^{-1} and the exclusion at 95% CL would be for the values smaller than 60 ps^{-1}. The plot for this result is shown in Appendix C.

5.3 Resolutions analysis

In this section the results are presented for the calculation of the resolution of different parameters (masses, momenta, vertex positions and proper time). All the histograms in this section have been fitted (χ^2 fit) with either a single or a double Gaussian. In the cases where a double Gaussian has been used, it has been assumed that the mean was equal for both curves, which means that five parameters are used in the fit. The plots and the results show the fraction of the area under each of the Gaussian used for the fit. The events plotted in all the histograms in this section are selected, untriggered events.

5.3.1 Masses resolutions

Figure 13 shows both the B_s and the D_s mass resolutions. The result for the resolutions, given by the fit using a single Gaussian function, are:

$$\sigma_{M_{B_s}} = 14.3 \text{ MeV}/c^2$$

$$\sigma_{M_{D_s}} = 5.30 \text{ MeV}/c^2$$

The second result shows that the tight mass cut correspond to $\sim 3\sigma$ on both side, which is not too tight as it could have been thought at first.

A double Gaussian was then used to get a better fit. The results found are (as shown in Fig. 13):

$$\begin{aligned} \sigma_{M_{B_s}} &= 12.1 \text{ MeV}/c^2 \ (71\%) \quad + \quad 20.3 \text{ MeV}/c^2 \ (29\%) \\ \sigma_{M_{D_s}} &= 3.72 \text{ MeV}/c^2 \ (40\%) \quad + \quad 6.47 \text{ MeV}/c^2 \ (60\%). \end{aligned}$$

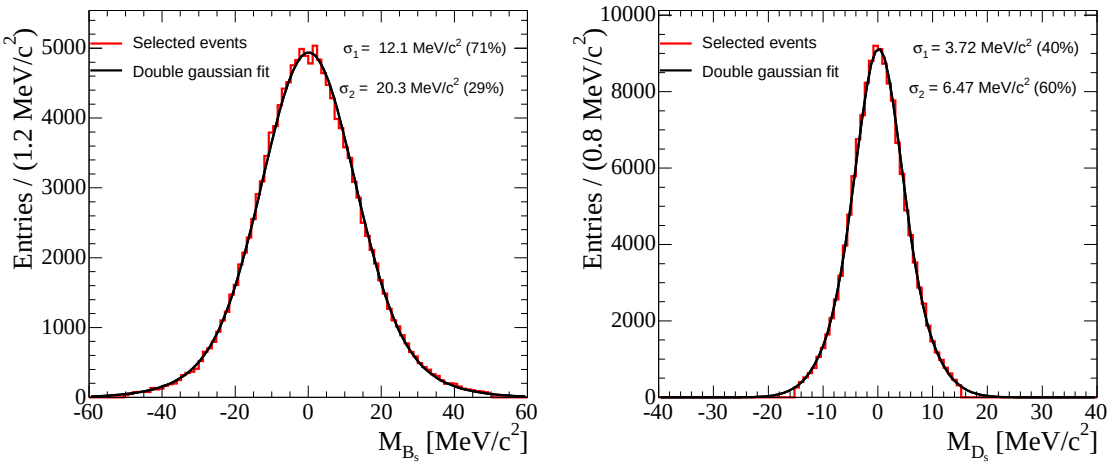

FIG. 13: B_s and D_s mass resolutions.

5.3.2 Momentum resolutions

The momentum resolutions (3 coordinates) for the B_s are shown in Fig. 14. A double Gaussian has been fitted on the distributions both for the x and y resolution but a triple Gaussian was needed for the z momentum resolution because of the bad fit with a double Gaussian. The results of the fit are:

$$\begin{aligned}
\sigma_{P_{x,B_s}} &= 11.9 \text{ MeV}/c \ (74\%) \quad + \quad 35.8 \text{ MeV}/c \ (26\%) \\
\sigma_{P_{y,B_s}} &= 11.6 \text{ MeV}/c \ (73\%) \quad + \quad 36.2 \text{ MeV}/c \ (27\%) \\
\sigma_{P_{z,B_s}} &= 118 \text{ MeV}/c \ (31\%) \quad + \quad 318 \text{ MeV}/c \ (46\%) \quad + \quad 867 \text{ MeV}/c \ (23\%).
\end{aligned}$$

5.3.3 Vertices position resolutions

Due to the large boost of the events in LHCb, the z-position of the primary vertex could have a bad resolution. Fig. 15 (a) show that this is not the case. Indeed, the resolution of this coordinate is

$$\sigma_{z_{PV}} = 27.7 \ \mu\text{m} \ (36\%) \quad + \quad 48.2 \ \mu\text{m} \ (51\%) \quad + \quad 104 \ \mu\text{m} \ (13\%).$$

This good resolution is due to the fact that the primary vertex is fitted with many tracks, including tracks with a large opening angle. Fig. 15 (b) and (c) show that the x and y coordinates of the primary vertex have a better resolution, which is as expected because of the low momentum in these directions:

$$\begin{aligned}
\sigma_{x_{\text{PV}}} &= 6.47 \ \mu\text{m} \ (73\%) \quad + \quad 13.0 \ \mu\text{m} \ (27\%) \\
\sigma_{y_{\text{PV}}} &= 6.35 \ \mu\text{m} \ (76\%) \quad + \quad 12.8 \ \mu\text{m} \ (24\%).
\end{aligned}$$

The resolution on the position of the secondary vertex (i.e. the B_s-decay vertex)

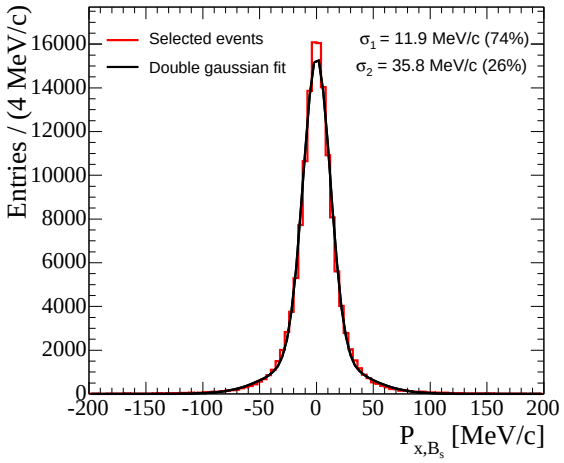

(a) B_s momentum x-resolution,

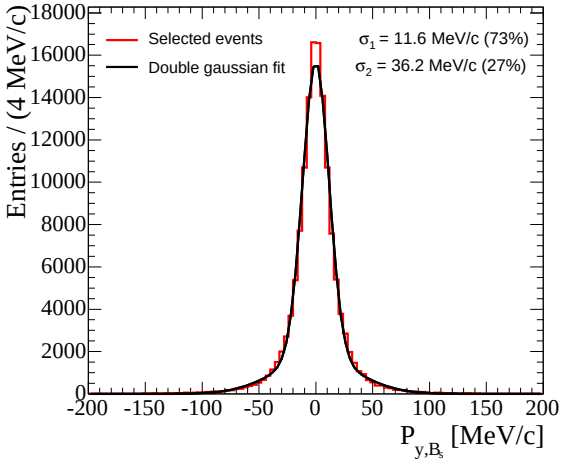

(b) B_s momentum y-resolution,

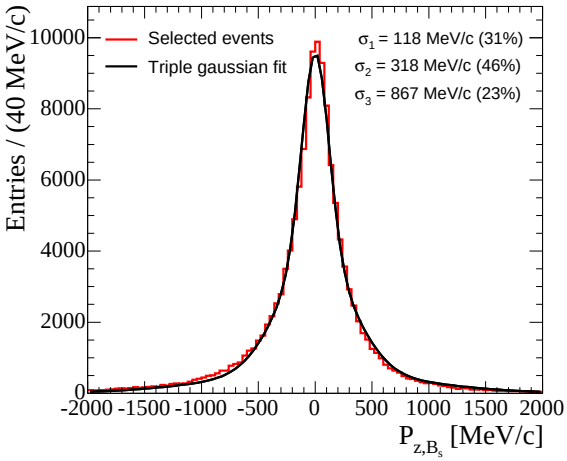

(c) B_s momentum z-resolution.

FIG. 14: Resolutions on the B_s momentum

is not as good as that for the primary vertex (Fig. 15 (d), (e) and (f)):

$$\begin{aligned}
\sigma_{x_{B_s}} &= 11.5\ \mu\text{m}\ (72\%) \quad + \quad 24.7\ \mu\text{m}\ (28\%) \\
\sigma_{y_{B_s}} &= 10.1\ \mu\text{m}\ (71\%) \quad + \quad 24.4\ \mu\text{m}\ (29\%) \\
\sigma_{z_{B_s}} &= 105\ \mu\text{m}\ (41\%) \quad + \quad 280\ \mu\text{m}\ (41\%) \quad + \quad 780\ \mu\text{m}\ (18\%).
\end{aligned}$$

This is due to the fact that particles are mainly produced under small angles in the forward direction.

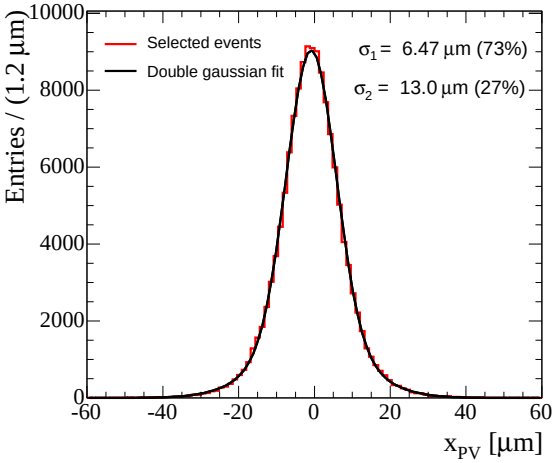

(a) Primary vertex x-resolution,

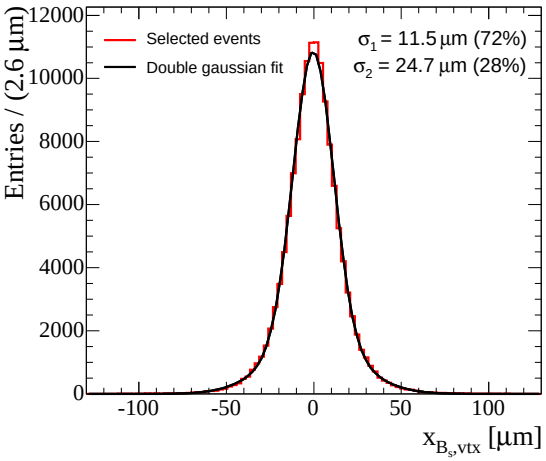

(d) B_s-decay vertex x-resolution,

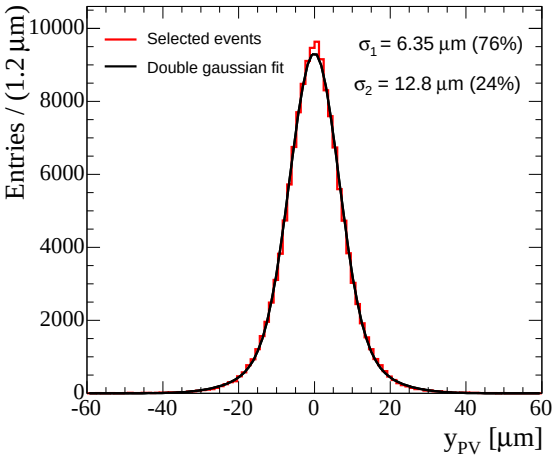

(b) Primary vertex y-resolution,

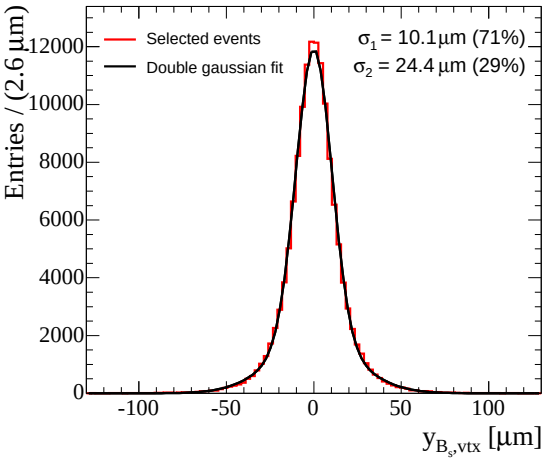

(e) B_s-decay vertex x-resolution,

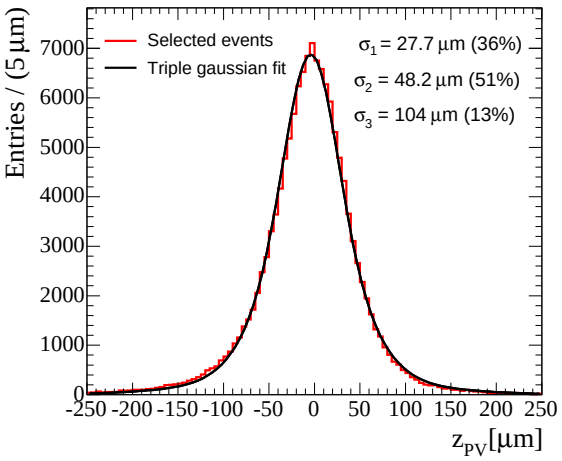

(c) Primary vertex z-resolution,

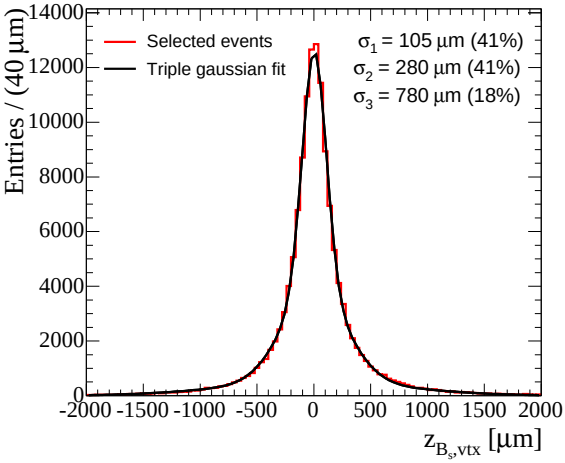

(f) B_s-decay vertex z-resolution.

FIG. 15: Resolutions on the primary vertex and the B_s-decay vertex positions

5.3.4 Proper time resolution

The proper time τ is calculated using an algorithm called LifeTimeFitter. This algorithm performs a constrained fit which parametrises a particle's flight as

$$\overrightarrow{\text{Decay Vertex}} = \overrightarrow{\text{Origin Vertex}} + \frac{\overrightarrow{\text{Momentum}} \cdot \tau}{\text{Mass}}$$
$$\Longrightarrow \qquad \tau = \frac{\text{Mass} \cdot \|(\overrightarrow{\text{Decay Vertex}} - \overrightarrow{\text{Origin Vertex}})\|}{\|\overrightarrow{\text{Momentum}}\|} \tag{36}$$

and which minimises a χ^2 to obtain τ given a particle (and thus its measured decay vertex and measured momentum) and an origin vertex.

Figure 16 shows the distribution of the proper time. Fitting this distribution (in the range [2,12] ps) with an exponential curve gives a proper time

$$\tau = (1.455 \pm 0.006) \text{ ps}$$

which is consistent (1σ) with the value used in the generation

$$\tau_{MC} = 1.461 \text{ ps}.$$

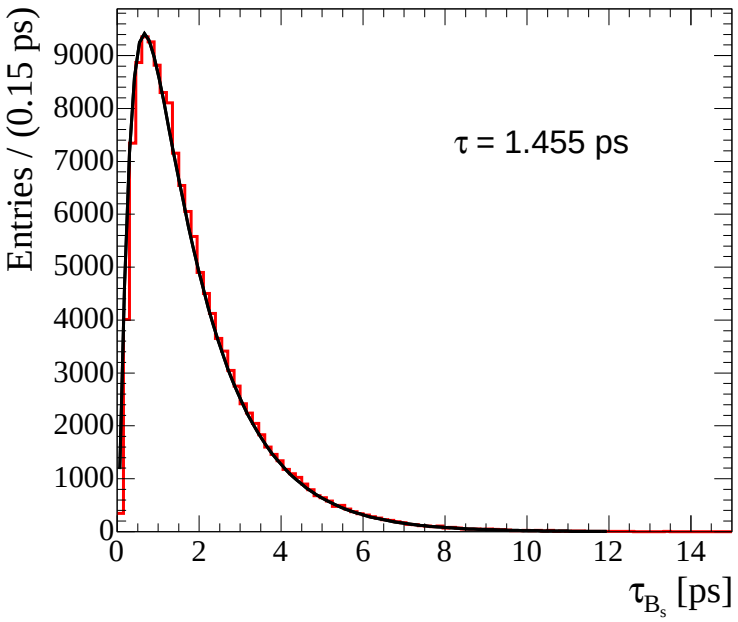

FIG. 16: τ_{B_s} distribution.

The black solid-curve in Fig. 16 has been obtained by fitting to the distribution a function made of the acceptance function (see Section 5.5) with the fit parameters calculated multiplied by the exponential with the parameter calculated above ($\tau =$ 1.486 ps). The fit shows that the exponential describes well the right tail of the

distribution and the acceptance function is a good description of the falloff of the distribution for small proper times.

Using the Monte Carlo true lifetime, the resolution on the proper time can be plotted. Fig. 17 shows the resolution on the proper time. The fit done with a double Gaussian shows that this resolution is equal to

$$\sigma_{\tau_{B_s}} = 29.7 \text{ fs } (63\%) \quad + \quad 56.7 \text{ fs } (37\%).$$

A single value can be found for this resolution, using

$$\sigma = \sqrt{f_1\sigma_1^2 + f_2\sigma_2^2} = 41.8 \text{ fs}$$

which has been used for the plot of the sensitivity to ΔM_s and where f_i and σ_i are respectively the fraction of the events described by the i^{th} Gaussian and its standard deviation.

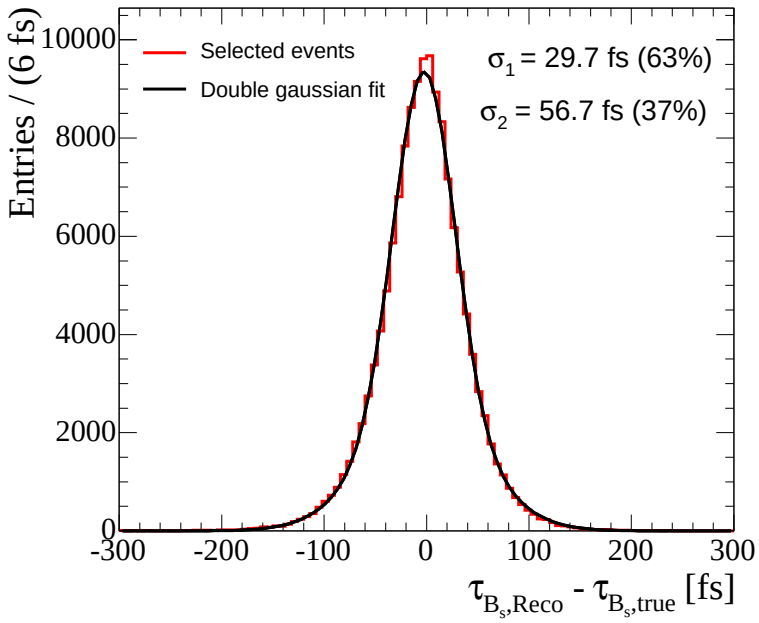

FIG. 17: τ_{B_s} resolution.

5.3.5 Decomposition of Proper time resolution using the MC truth

Equation (36) shows that the proper time is calculated using four different parameters: the origin vertex, the decay vertex, the momentum and the mass of the B_s. The resolution on each of these 4 parameters (10 parameters if the separate coordinates are counted) has an influence on the resolution of the proper time. This section will show the influence of each of these parameters using the MC Truth. The proper time of each reconstructed B_s will be calculated four times using at each step

the MC Truth of the four parameters except for one (which will be called All true but one).

Figure 18 (a) and (b) shows the proper time resolution using the MC Truth for all parameters but the reconstructed mass (left plot) and all true parameters but the momentum (3 coordinates, right plot). These histograms show that the resolution on the proper time is not too much affected by these parameters:

$$\begin{aligned} \sigma_{\tau/M_{B_s}} &= 3.08 \text{ fs } (71\%) \quad + \quad 9.84 \text{ fs } (29\%) \\ \sigma_{\tau/M_{P_s}} &= 3.11 \text{ fs } (71\%) \quad + \quad 10.5 \text{ fs } (29\%). \end{aligned}$$

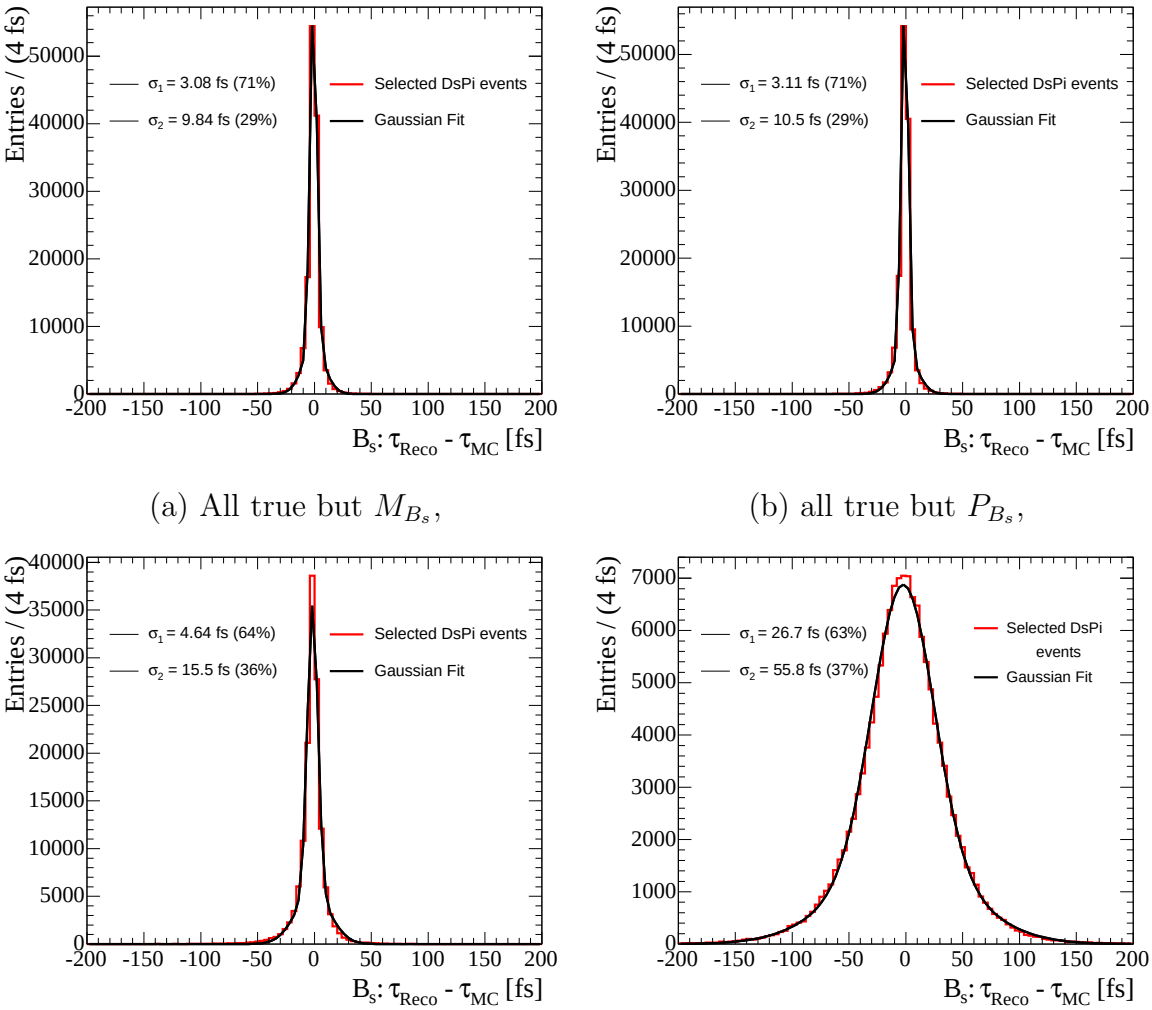

(a) All true but M_{B_s},

(b) all true but P_{B_s},

(c) all true but primary vertex,

(d) all true but B_s decay vertex.

FIG. 18: Decomposition of the resolution on τ_{B_s} using the MC truth

Figure 18 (c) and (d) shows the proper time resolution using the MC Truth for all parameters but the reconstructed primary vertex (B_s origin vertex) and all true but the reconstructed secondary vertex (B_s decay vertex). Again, the primary vertex

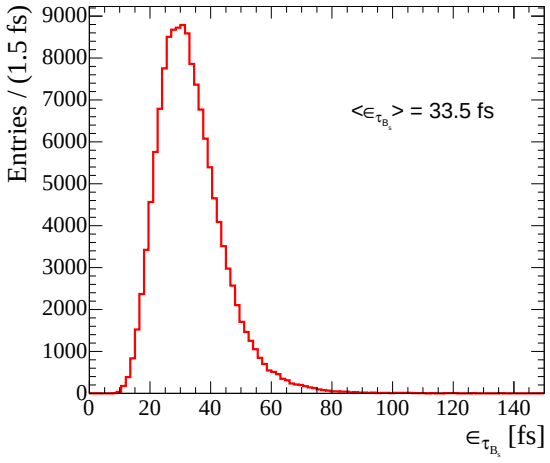

FIG. 19: Error on τ_{B_s}.

doesn't seem to have much influence on the proper time resolution. The resolution on the proper time is by far dominated by the resolution of the secondary vertex. This is actually not a surprise as we recall that the resolution on the B_s-decay vertex was not as good as the primary one, due to the boost and the smaller number of tracks to reconstruct this vertex.

$$\begin{aligned} \sigma_{\tau/PV} &= 4.64 \text{ fs } (64\%) \quad + \quad 15.5 \text{ fs } (36\%) \\ \sigma_{\tau/B_s} &= 26.7 \text{ fs } (63\%) \quad + \quad 55.8 \text{ fs } (37\%). \end{aligned}$$

5.4 Proper time pull analysis

The error on the proper time is calculated on an event-per-event basis using the LifeTimeFitter algorithm. The per-event error on the proper time is estimated using the momentum and vertices covariance matrices. This algorithm returns both the proper time and its error. Fig. 19 shows the distribution of this calculated error. It is interesting to see that the errors are never equal to zero (the distribution starts only at 10 fs), the mean is

$$\langle \sigma_{\epsilon_\tau} \rangle = 33.5 \text{ fs},$$

which is consistent with the core resolution of ∼30 fs of the proper time. It is also interesting to see that the spectrum is quite wide.

The first part of this chapter will show the calculation of the pull on the proper time and the second part will show the dependence of this pull on various parameters.

5.4.1 Calculation of proper time pull

The pull on a parameter is a measurement of how well the errors on the studied parameter are estimated. The pull on the proper time is actually the standard

deviation (σ) of the distribution of

$$\frac{\tau_{B_s,\text{reco}} - \tau_{B_s,\text{true}}}{\sigma_{\tau_{B_s}}}$$

where $\sigma_{\tau_{B_s}}$ is the "per-event error" on the proper time. Thus if the error is well estimated, the pull should be close to 1 and the mean of the distribution compatible with 0.

Figure 20 shows this distribution for the selected, untriggered events. The fitted pull is

$$\text{Pull} \simeq 1.2 \pm 0.0$$

which means that the errors on the proper time are under-estimated. The mean of the histogram is equal to -0.074 ± 0.003 which means that the errors are in average biased to negative values, which also corresponds to an under-estimation of the errors.

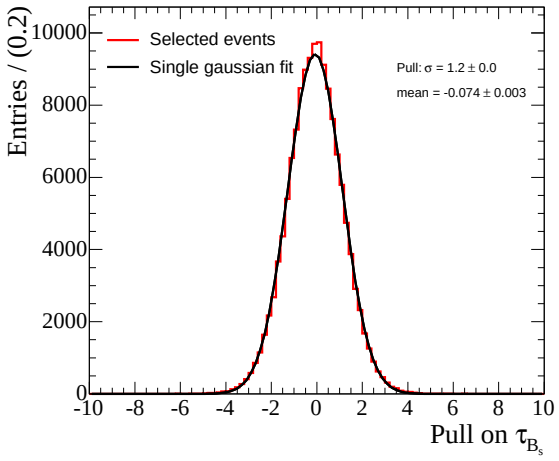

FIG. 20: Pull on τ_{B_s}.

5.4.2 Dependence of proper time pull on various parameters

For the following figures, the pull has been calculated in each case by separating the whole sample of selected events in five bins of the studied parameter (P_{B_s}, p_{T,B_s}, τ_{B_s}, $\sigma_{\tau_{B_s}}$, closest distance approach of the D_s and the bachelor (δ, see Eq. 37), opening angle between the D_s and the bachelor directions (ϕ, see Eq. 38) and χ^2 of the B_s decay vertex). Then, the distributions obtained (for the selected and untriggered events) are fitted independently and the σ of each Gaussian fit is plotted

in the middle of the bin.

$$\delta = \left| \frac{(\overrightarrow{P}_{D_s} \times \overrightarrow{P}_H) \cdot (\overrightarrow{D_{s,\text{Pt. on tr.}}} - \overrightarrow{H_{\text{Pt. on tr.}}})}{\left\|(\overrightarrow{P}_{D_s} \times \overrightarrow{P}_H)\right\|} \right| \quad (37)$$

$$\cos(\phi) = \frac{\overrightarrow{P}_{D_s} \cdot \overrightarrow{P}_H}{\left\|\overrightarrow{P}_{D_s}\right\| \cdot \left\|\overrightarrow{P}_H\right\|} \quad (38)$$

where H is the bachelor pion and "Pt. on tr." means Point on Track which is the point on a track where the particle's momentum is assigned.

Figure 21 and 22 show the dependence of the pull on τ_{B_s} on the parameters listed above. These distributions show that the only two parameters that have an influence on the estimation of the errors are the B_s momentum and the opening angle between the two daughters of the B_s. Also the closest distance approach and the precision of the secondary vertex definition have an influence but smaller. The solid black lines drawn on these plots are not fitted through the data. They have been drawn to indicate the behaviour of the pull.

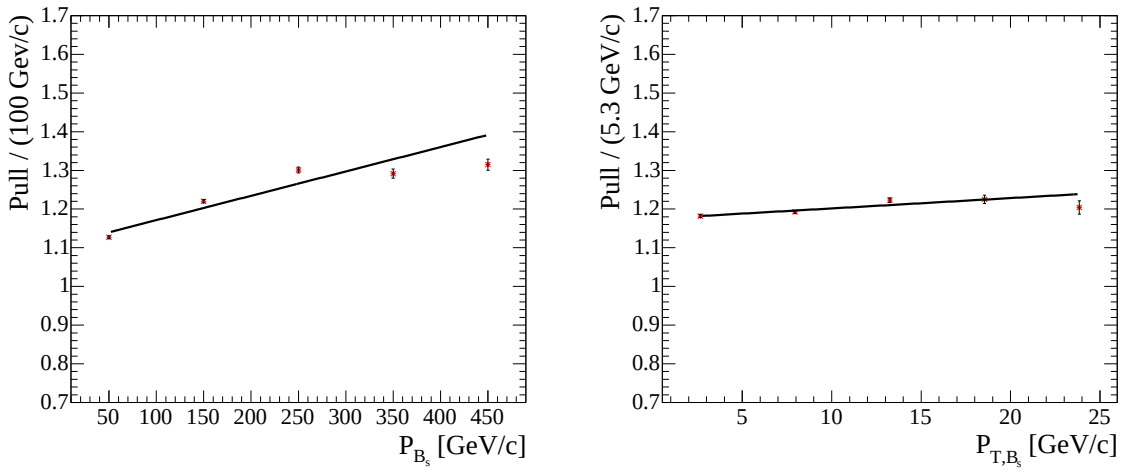

(a) Pull vs P_{B_s}, (b) Pull vs $p_{T_{B_s}}$.

FIG. 21: Dependence of τ_{B_s} pull on the B_s momentum and transverse momentum.

Figure 21 (a) shows that the larger the B_s momentum is, the more underestimated the errors on the proper time are.

Figure 22 (d) shows that for small opening angles between the D_s and the bachelor, the error are more underestimated than for large opening angles. This arises from the fact that the resolution on the secondary vertex is larger for smaller opening angles.

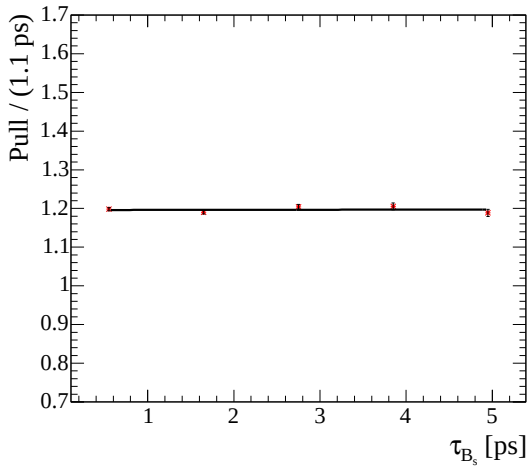

(a) Pull vs τ_{B_s},

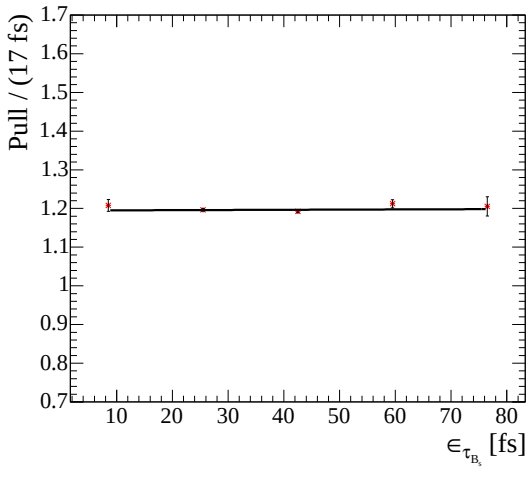

(b) Pull vs $\epsilon_{\tau_{B_s}}$,

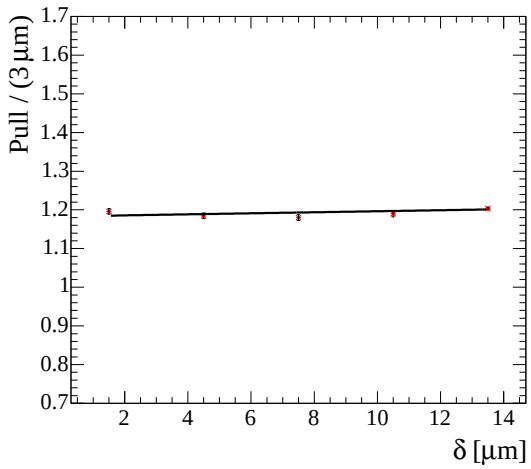

(c) Pull vs δ (Eq. (37)),

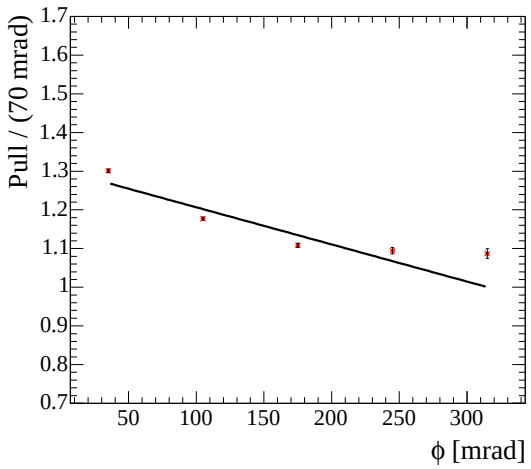

(d) Pull vs ϕ (Eq. (38)),

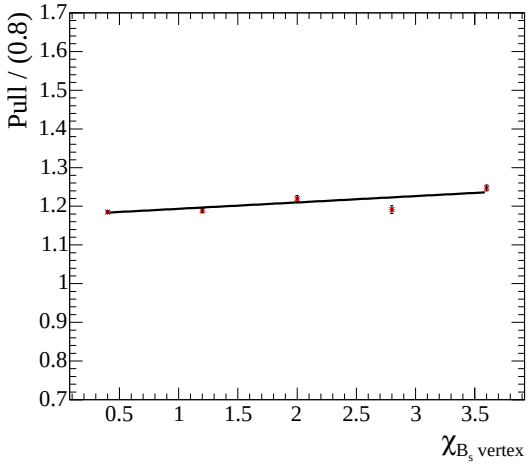

(e) Pull vs $\chi^2(B_s$ decay vertex).

FIG. 22: Dependence of τ_{B_s} pull on various parameters.

5.5 Acceptance analysis

In the selection criteria, events with small proper times are implicitely rejected when e.g. a detached secondary vertex is required. Thus the probability for a true event to be detected is not uniform and depends on the true proper time. This probability is described by the acceptance function. It corresponds to a time-dependent bin-per-bin selection efficiency. This acceptance is calculated by dividing bin-per-bin the distribution of the proper time of the B_s before selection by the distribution after selection. The behaviour of this new curve can be fitted by a time-dependent function:

$$\frac{a \cdot (b \cdot t_{\mathrm{MC}})^n}{(1 + (b \cdot t_{\mathrm{MC}})^n)} \cdot (1 + c \cdot t_{\mathrm{MC}}) \tag{39}$$

where there are four free parameters including the power and t_{MC} is the true MC time. The parameter a is a normalization factor, b and n parametrise the shape of the fit and c is the slope of the curve for large values of the proper time.

From Fig. 23, it is clearly visible that the efficiency tends to zero for small values of the proper time. This is due to the cuts on the flight significance and all cuts requiring a detached secondary vertex. In addition, it is due to the cut on $\cos(\theta_P)$ because for small proper times the decay length is not large enough to define the angle properly. For large proper time values, the behaviour is not well defined because of the limited statistics (large error bars).

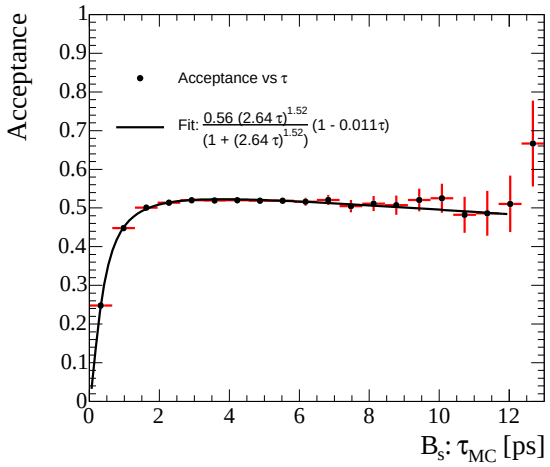

FIG. 23: Acceptance before triggers.

It still looks like the efficiency drops for large values of τ_{B_s} as the slope of the fitted function (the parameter c) is

$$c_{\text{No trig.}} = (-0.011 \pm 0.003)\ \text{ps}^{-1},$$

$$c_{\text{L0}} = (-0.0095 \pm 0.0046)\ \text{ps}^{-1},$$

$$c_{\text{L0 and L1}} = (-0.039 \pm 0.004)\ \text{ps}^{-1}.$$

The slope is not really significant before trigger (3.5σ) nor after L0 (2σ) but is quite significant after L1.

The low efficiency for small values of the proper time is even more visible after the triggers have been applied (especially L1). This is due to the cuts requiring large IP tracks. The surprising fact is that the L1 trigger biases a lot the acceptance for large values of the proper time.

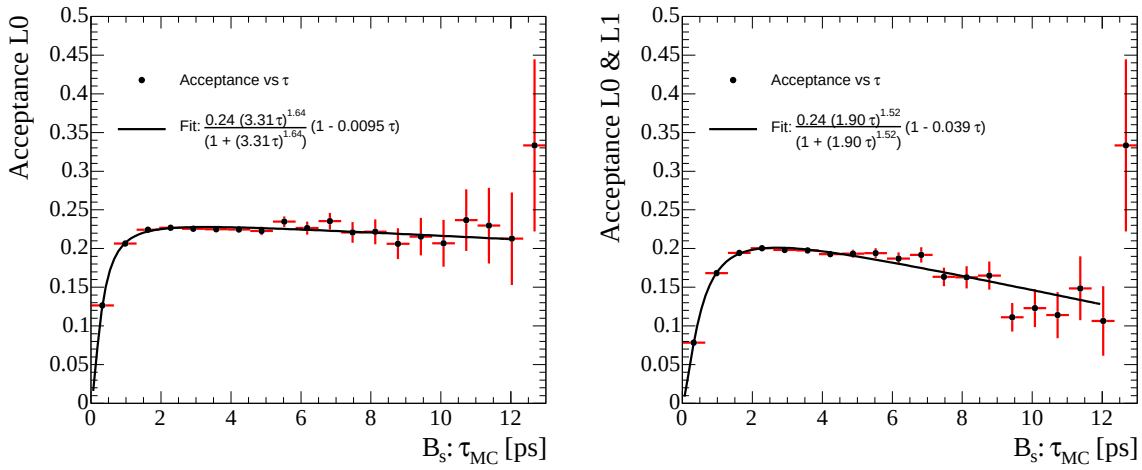

(a) Acceptance after L0, (b) Acceptance after L0 and L1.

FIG. 24: Acceptance after L0 and after L0 and L1 triggers.

6 Conclusion

This study was dedicated to the analysis of the $B_s^0 \to D_s^- \pi^+$ decay. This decay is used to extract the physics parameters ΔM_s, $\Delta\Gamma_s$ and the wrong tag fraction ω.

The purpose of this study was to redo a complete analysis of this decay on the Monte Carlo data produced with the new software versions of the generation, simulation and reconstruction.

A set of selection cuts was found resulting in a high signal selection efficiency (high annual yield), while keeping a small background (composed of $b\bar{b}$ events). The results obtained for the number of selected and triggered events per year is:

$$N_{\text{phys}} = (111.4 \pm 0.5)\text{k events}$$

compared to $N_{\text{phys}} = 80$k at the time of the TDR. The background-to-signal ratio was calculated and a value of

$$\left(\frac{B}{S}\right)^{\text{inclusive-}b\bar{b}}_{B_s^0 \to D_s^- \pi^+} = 0.83 \pm 0.09$$

was obtained. Table 12 shows a summary of the individual efficiencies, the annual signal yield and the background-to-signal ratio.

TAB. 12: Summary of the signal efficiencies, the untagged annual signal yield and the background-over-signal ratio for the DC04 $B_s^0 \to D_s^- \pi^+$ data.

Factors (in %) forming ϵ_{tot} (in %) $\epsilon_{\rm tot} = \epsilon_{\rm det} \times \epsilon_{\rm rec/det} \times \epsilon_{\rm sel/sec} \times \epsilon_{\rm trg/sel}$					Assumed $\rm BR_{vis}$ (in 10^{-6})	Annual signal yield	B/S ratio from incl. $b\bar{b}$ back.
$\epsilon_{\rm det}$	$\epsilon_{\rm rec/det}$	$\epsilon_{\rm sel/rec}$	$\epsilon_{\rm trg/sel}$	$\epsilon_{\rm tot}$			
6.255	78.74	25.24	36.90	0.4586	120	111.4k	0.83

The wrong tag fraction obtained is $\omega = (33.53 \pm 0.15)\%$ while the 5σ measurement of ΔM_s was found to be possible up to a value of $\Delta M_s = 46$ ps^{-1}. The values smaller than 58 ps^{-1} can be excluded with a CL of 95%.

Finally the proper time resolution and the pull on the proper time were investigated. The B_s^0 proper time was fitted with a double Gaussian, giving a resolution of

$$\sigma_{\tau_{B_s}} = 29.7 \text{ fs } (63\%) \quad + \quad 56.7 \text{ fs } (37\%).$$

The proper time resolution is dominated by the resolution on the position of the B_s-decay vertex. The proper time pull was found to be equal to 1.2, which means that the errors on the B_s proper time are under-estimated. This pull is dependent on the momentum of the B_s (the higher the momentum the higher the pull) as well as on the opening angle between the D_s and the bachelor pion (the higher the opening angle the lower the pull).

Acknowledgments

I wish to thank Olivier Schneider for welcoming me to the LPHE, for suggesting this analysis and for his help when it was needed. I am also really thankful to my two assistants Luis Fernández and Jeroen van Hunen for all the time they spent helping me out with the coding, the writing and the thinking in this study. I am also indebted to Benjamin Carron for the numerous problems with Root he solved for me. Finally, I am grateful to Cédric Potterat and François Gigante for all the time spent together motivating and supporting each other.

A L1 trigger cuts

The cuts applied for the Level-1 trigger used in this analysis are presented in Table 13. These cuts might change again before the real experiment runs as both the Level-1 trigger and the High Level Trigger are still being improved. These cuts still give an idea of what will be done.

TAB. 13: Summary of the cuts used in Level-1 trigger.

Cut	Requirement		
$p_{T,1}$, $p_{T,2}$	$\log(p_{T,1}) + \log(p_{T,2})$	$>$	13.55
Single μ	$p_{T,\mu}$	$>$	1950 MeV/c
Dimuon	M_{dimuon}	$>$	500 MeV/c^2
AND	$\text{IP}_{\text{dimuon}}$	$>$	0.05 mm
J/ψ	$\lvert M_{J/\psi} - M_{\text{MC } J/\psi}\rvert$	$<$	500 MeV/c^2
OR	$M_{J/\psi}$	$>$	$M_{\text{MC } B_d}$ - 500 MeV/c^2
Electron	$E_{T,e}$	$>$	3450 MeV/c
AND	$\log(p_{T,1}) + \log(p_{T,2})$	$>$	12.72
Photon	$E_{T,\gamma}$	$>$	3150 MeV/c
AND	$\log(p_{T,1}) + \log(p_{T,2})$	$>$	12.72

B Tagging information

These are the informations given by the tagging algorithm before trigger, after L0 and after L0 and L1.

Here are a few definitions to better understand the tables:

- πs: same side pion,
- Ks: same side kaon,
- OS: opposite side tagging,
- SS: same side tagging.

Tab. 14: Summary of the tagging informations on selected events before trigger.

Category	ϵ_{eff} in %	ϵ_{tag} in %	ω in %
μ only	0.38±0.02	4.10±0.03	34.9±0.4
e only	0.30±0.02	1.67±0.02	28.7±0.5
K only	0.74±0.03	16.46±0.06	39.4±0.2
μ + k	0.19±0.01	1.07±0.02	29.1±0.7
e + K	0.11±0.01	0.42±0.01	24.8±1.0
vertex only	0.20±0.01	11.35±0.05	43.3±0.2
πs/Ks	1.26±0.03	12.07±0.05	33.8±0.2
μ + Ks	0.13±0.01	0.57±0.01	26.1±0.9
e + Ks	0.07±0.01	0.22±0.01	21.6±1.3
K + Ks	0.38±0.02	2.48±0.02	30.4±0.4
μ+K+Ks	0.04±0.01	0.56±0.01	36.7±1.0
e+K+Ks	0.03±0.00	0.20±0.01	31.6±1.6
muons	0.70±0.02	6.30±0.04	33.3±0.3
electrons	0.50±0.02	2.51±0.02	27.7±0.4
OS kaons	1.34±0.03	21.19±0.07	37.4±0.2
SS π/k	1.87±0.04	16.09±0.06	32.9±0.2
Tagging efficiency		ϵ_{tag} =	51.17 ± 0.09
Wrong tag fraction		ω =	36.34 ± 0.09
Effective comb. tag. eff.		ϵ_{eff} =	3.82 ± 0.08

TAB. 15: Summary of the tagging informations on selected events after L0.

Category	ϵ_{eff} in %	ϵ_{tag} in %	ω in %
μ only	0.86±0.04	7.51±0.06	33.1±0.4
e only	0.32±0.02	1.82±0.03	29.0±0.8
K only	0.84±0.04	14.79±0.09	38.1±0.3
μ + K	0.42±0.03	1.87±0.03	26.3±0.7
e + K	0.13±0.01	0.45±0.02	23.1±1.5
vertex only	0.23±0.02	10.50±0.07	42.6±0.3
πs/Ks	1.58±0.06	12.65±0.08	32.3±0.3
μ + Ks	0.28±0.02	1.06±0.02	24.2±1.0
e + Ks	0.10±0.01	0.28±0.01	20.2±1.8
K + Ks	0.47±0.03	2.51±0.04	28.3±0.7
μ+K+Ks	0.09±0.01	0.98±0.02	35.0±1.1
e+K+Ks	0.03±0.01	0.20±0.01	29.2±2.4
muons	1.60±0.06	11.43±0.08	31.3±0.3
electrons	0.58±0.03	2.76±0.04	27.1±0.6
OS kaons	1.80±0.06	20.81±0.10	35.3±0.2
SS π/k	2.50±0.07	17.68±0.09	31.2±0.2
Tagging efficiency		ϵ_{tag} =	54.64 ± 0.14
Wrong tag fraction		ω =	34.34 ± 0.13
Effective comb. tag. eff.		ϵ_{eff} =	5.36 ± 0.15

TAB. 16: Summary of the tagging informations on selected events after L0&L1.

Category	ϵ_{eff} in %	ϵ_{tag} in %	ω in %
μ only	1.01±0.05	8.29±0.08	32.5±0.4
e only	0.39±0.03	1.99±0.04	28.0±0.9
K only	1.02±0.06	14.98±0.10	37.0±0.3
μ + K	0.50±0.04	2.12±0.04	25.6±0.8
e + K	0.16±0.02	0.52±0.02	22.4±1.6
vertex only	0.27±0.03	10.82±0.09	42.2±0.4
πs/Ks	1.63±0.07	12.14±0.09	31.7±0.4
μ + Ks	0.33±0.03	1.18±0.03	23.4±1.1
e + Ks	0.12±0.02	0.31±0.02	19.1±2.0
K + Ks	0.52±0.04	2.52±0.04	27.3±0.8
μ+K+Ks	0.10±0.02	1.07±0.03	34.4±1.3
e+K+Ks	0.05±0.01	0.21±0.01	26.7±2.7
muons	1.89±0.07	12.66±0.10	30.7±0.4
electrons	0.70±0.04	3.03±0.05	26.0±0.7
OS kaons	2.16±0.08	21.43±0.12	34.1±0.3
SS π/k	2.68±0.09	17.44±0.11	30.4±0.3
Tagging efficiency		ϵ_{tag} =	56.17 ± 0.18
Wrong Tag fraction		ω =	33.53 ± 0.15
Effective comb. tag. eff.		ϵ_{eff} =	6.10 ± 0.19

C Sensitivity to ΔM_s

Figure 25 shows the sensitivity to ΔM_s which is calculated using Eq. (35) with the numbers of the TDR:

- $\epsilon_{\text{eff}} = 8.45\%$,
- $N_{\text{phys}} = 82\text{k}$,
- $\sigma_\tau = 46.3$ fs ($\sigma_\tau = \sqrt{69\% \cdot (33\text{ fs})^2 + 31\% \cdot (67\text{ fs})^2}$).

This plot shows that a 5σ measurement is possible up to 45 ps^{-1} while the values smaller than 56 ps^{-1} can be excluded with a 95% CL.

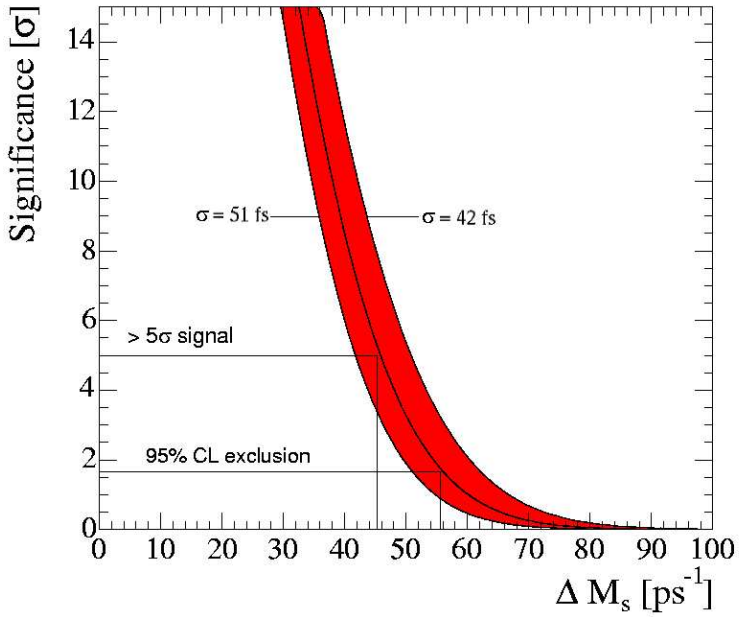

FIG. 25: The one year sensitivity to ΔM_s for a proper time resolution of 46.3 fs $\pm$ 10% using the numbers of the TDR.

Figure 26 shows the significance of ΔM_s which is calculated using Eq. (35) with the combined effective tagging efficiency obtained with the new tagging algorithms based on neural nets ($\epsilon_{\text{eff}} = 9.2\%$). This plot shows that a 5σ measurement can be obtained up to 48 ps^{-1} and the values smaller than 60 ps^{-1} can be excluded with a 95% CL.

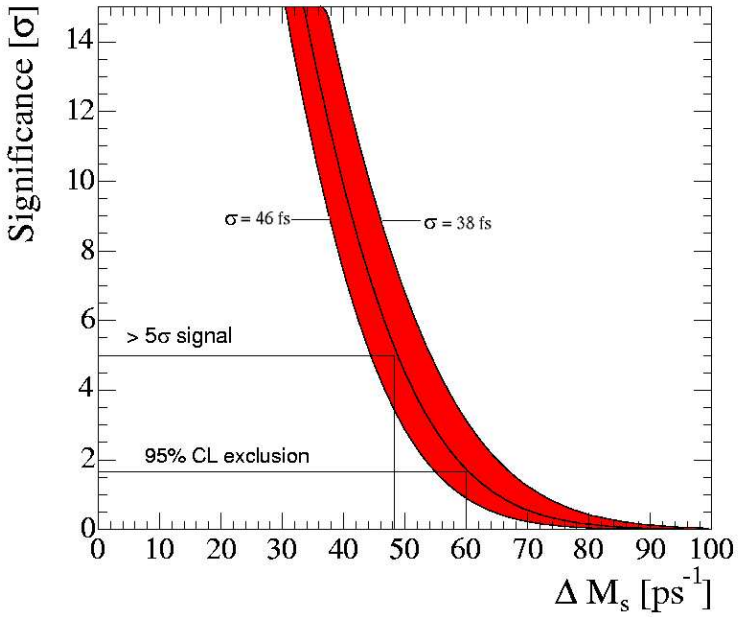

FIG. 26: The one year sensitivity to ΔM_s for a proper time resolution of 42.0 fs $\pm$ 10% using the upgraded flavour tagging algorithm for a better combined effective tagging efficiency.

References

[1] *Evidence for the 2 π Decay of the K_2^0 Meson*, J.H. Christenson *et al.*, Phys. Rev. Lett. **13**, 138 (1964)

[2] *Flavour Physics and CP violation*, Robert Fleischer, May 11th, 2004, CERN-PH-TH/2004-085,
[http://arxiv.org/abs/hep-ph/0405091]

[3] *Parametrisation of the Kobayashi-Maskawa Matrix*, L. Wolfenstein, Phys. Rev. Lett. **51**, 1945 (1983)

[4] *Sensitivities to the $B_s^0 - \bar{B}_s^0$ Mixing Parameters using $\bar{b} \to \bar{c}c\bar{s}$ Quark Transitions at LHCb*, Luis Fernández, Swiss Physical Society meeting talk, Neuchatel, March 3rd, 2004,
[http://lphe.epfl.ch/publications/2004/luis_sps.pdf]

[5] *$B_s^0 \to D_s^{\pm} K^{\mp}$ and $B_s^0 \to D_s^- \pi^+$ event selection*, A. Golutvin, R. Hierck, J. van Hunen, M.Prokudin, R. White, September 11th, 2003, CERN-LHCb/2003-127, PHYS

[6] *The sensitivity for ΔM_s and $\gamma + \phi_s$ from $B_s^0 \to D_s^- \pi^+$ and $B_s^0 \to D_s^{\pm} K^{\mp}$ decays*, R. Hierck, J. van Hunen, M. Merk, October 3rd, 2003, CERN-LHCb/2003-103, PHYS

[7] LHCb Technical Proposal, A Large Hadron Collider Beauty Experiment for Precision Measurements of CP Violation and Rare Decays, CERN-LHCC-98-004

[8] LHCb Technical Design Report 9, Reoptimised Detector Design and Performance, CERN-LHCC-2003-030.

[9] LHCb Technical Design Report 3, RICH, CERN-LHCC-2000-037

[10] LHCb Technical Design Report 2, Calorimeters, CERN-LHCC-2000-036

[11] LHCb Technical Design Report 10, Trigger System, CERN-LHCC-2003-031

[12] *L1 and HLT generic*, J. A. Hernando, LHCC Comprehensive Review, January 31st, 2005

[13] *Trigger algorithms and physics: introduction*, O. Schneider, LHCC Comprehensive Review, January 31st, 2005

[14] *Specific HLT*, P. Koppenburg, LHCC Comprehensive Review, January 31st, 2005

[15] *LHCb Flavour Tagging Performance*, M. Calvi, O. Dormond, M. Musy, September 15th, 2003, LHCb-2003-115,
[http://doc.cern.ch//archive/electronic/cern/others/LHB/public/lhcb-2003-115.pdf

[16] Pythia 6.2 - Physics and Manual, hep-ph/0108264, LU TP 01-21 (second edition), April 2002

[17] Gaudi, Gauss, EvtGen, Geant 4, Brunel - The LHCb computing framework, The LHCb B Generator Program, The LHCb Simulation Program and The LHCb Reconstruction Program,
[http://lhcb-comp.web.cern.ch/lhcb-comp/]

[18] DaVinci - The LHCb Analysis Program,
[http://lhcb-comp.web.cern.ch/lhcb-comp/Analysis/].

[19] LoKi - Loops & Kinematics, Smart & Friendly C++ Physics Analysis Toolkit, Vanya Belyaev

[20] Root - An Object-Oriented Data Analysis Framework,
[http://root.cern.ch/]

[21] Personal discussion with M. Cattaneo, P. Charpentier, T. Ruf, O. Schneider and V. Vagnoni, December 2004 - January 2005

[22] The Review of Particle Physics, S. Eidelman *et al.*, Particle Data Group, Phys. Lett. B 592, 1 (2004),
[http://pdg.lbl.gov/]

[23] *The new Efficiency algorithms*, C. Jacoby, P. Igo-Kemenes, September 29th, 2004, LHCb/2004-080, COMP,
[lphe.epfl.ch/publications/2004/MCEffNoteMaster.pdf]

[24] *New Developments on Flavour Tagging*, Marta Calvi, LHCC Comprehensive Review, January 31st, 2005